Article

Cell Reports

Evolutionary Remodeling of Bacterial Motility Checkpoint Control

Graphical Abstract

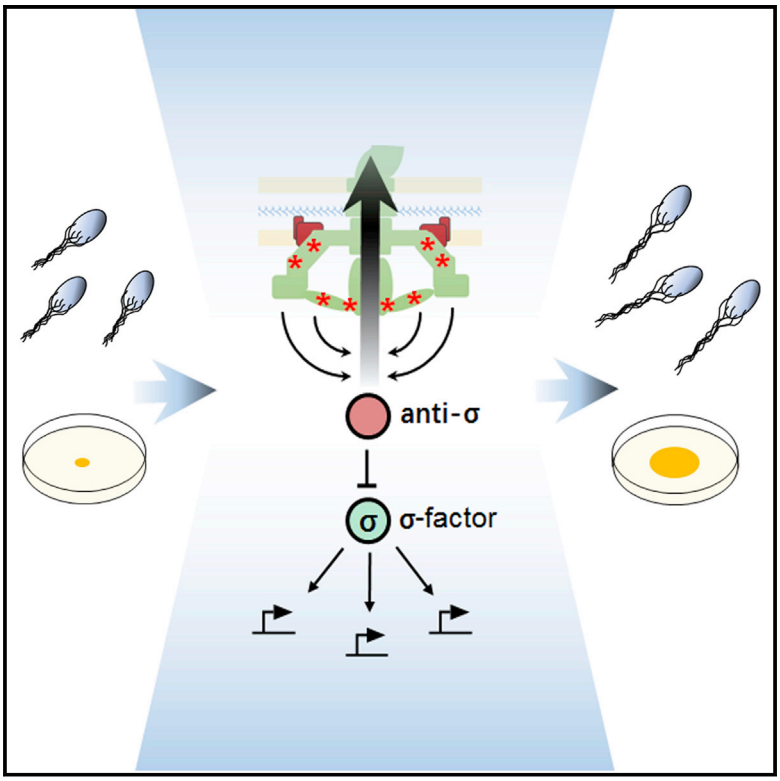

Authors

Bin Ni, Bhaswar Ghosh, Ferencz S. Paldy, Remy Colin, Thomas Heimerl, Victor Sourjik

Correspondence

victor.sourjik@synmikro.mpi-marburg.mpg.de

In Brief

Ni et al. use experimental evolution to investigate remodeling of bacterial motility under selection. Their study reveals a key role of the checkpoint control of flagellar gene expression in motility evolution. Bow-tie topology of the checkpoint control facilitates evolutionary tuning of the trade-off between motility and growth.

Highlights

- Multiple mutations enhance swimming behavior under selection
- A universal trade-off relationship between motility and growth is observed
- Checkpoint remodeling provides a mechanism of evolutionary adaptation
- Bow-tie topology facilitates evolvability of the motility network

Ni et al., 2017, Cell Reports *18*, 866–877
January 24, 2017
http://dx.doi.org/10.1016/j.celrep.2016.12.088

CellPress

OPEN ACCESS
CellPress

Cell Reports
Article

Evolutionary Remodeling of Bacterial Motility Checkpoint Control

Bin Ni,[1] Bhaswar Ghosh,[1] Ferencz S. Paldy,[2] Remy Colin,[1] Thomas Heimerl,[3] and Victor Sourjik[1,2,4,*]
[1]Max Planck Institute for Terrestrial Microbiology and LOEWE Center for Synthetic Microbiology (SYNMIKRO), Marburg 35043, Germany
[2]Zentrum für Molekulare Biologie der Universität Heidelberg, DKFZ-ZMBH Alliance, Heidelberg 69120, Germany
[3]LOEWE Center for Synthetic Microbiology (SYNMIKRO), Philipps-Universität Marburg, Marburg 35043, Germany
[4]Lead Contact
*Correspondence: victor.sourjik@synmikro.mpi-marburg.mpg.de
http://dx.doi.org/10.1016/j.celrep.2016.12.088

SUMMARY

Regulatory networks play a central role in the relationship between genotype and phenotype in all organisms. However, the mechanisms that underpin the evolutionary plasticity of these networks remain poorly understood. Here, we used experimental selection for enhanced bacterial motility in a porous environment to explore the adaptability of one of the most complex networks known in bacteria. We found that the resulting phenotypic changes are mediated by adaptive mutations in several functionally different proteins, including multiple components of the flagellar motor. Nevertheless, this evolutionary adaptation could be explained by a single mechanism, namely remodeling of the checkpoint regulating flagellar gene expression. Supported by computer simulations, our findings suggest that the specific "bow-tie" topology of the checkpoint facilitates evolutionary tuning of the cost-benefit tradeoff between motility and growth. We propose that bow-tie regulatory motifs, which are widespread in cellular networks, play a general role in evolutionary adaptation.

INTRODUCTION

Global regulatory networks control most cellular decisions, including differentiation, stress response, and environmental adaptation. These networks frequently have a specific "bow-tie" organization where multiple inputs and outputs are connected to a core process or a regulator (Csete and Doyle, 2004). In bacteria, one of the most common global regulatory motifs comprises a sigma factor—a promoter-specific subunit of the bacterial RNA polymerase—and an anti-sigma factor that binds and inhibits the sigma factor (Österberg et al., 2011; Paget, 2015). The multi-input structure of these motifs allows them to integrate a variety of stimuli that control stress responses (Hengge, 2009) and developmental checkpoints (Rudner and Losick, 2001).

One of the best-studied sigma/anti-sigma factor checkpoints is involved in the control of flagellar biosynthesis (Chilcott and Hughes, 2000; Mukherjee and Kearns, 2014). In *Escherichia coli* and other bacterial species, flagellar genes are organized in a hierarchical regulatory network of three classes based on their order of expression and common transcriptional regulation (Aldridge and Hughes, 2002; Chevance and Hughes, 2008; Chilcott and Hughes, 2000; Kalir et al., 2001) (Figure 1A). Altogether, this network encodes more than 40 proteins that are necessary for flagellar motility and chemotaxis (Minamino and Imada, 2015; Typas and Sourjik, 2015). At the upper level of this regulatory hierarchy is the class I master regulator that is formed by two polypeptides, FlhD and FlhC. It activates class II genes that encode structural components and assembly factors of the flagellar hook-basal body (HBB) complex and of the export apparatus required for biogenesis of flagellar filament. Two other class II genes encode the sigma factor σ^{28} (FliA) and the anti-σ^{28} factor (FlgM). At first, both polypeptides are coexpressed, but σ^{28} is inhibited by binding to FlgM. Upon HBB completion, however, FlgM is secreted from the cell through the flagellar export apparatus to release free σ^{28}. This activates expression of σ^{28}-controlled (class III) genes that encode the subunit of the flagellar filament (FliC), stator components of the flagellar motor (MotA and MotB), as well as the chemotaxis pathway (Hughes et al., 1993). Notably, *flgM*, *fliA*, and a number of genes that are required for flagellar assembly possess both class II and class III promoters, and are therefore referred to as class II+III genes (Chevance and Hughes, 2008; Chilcott and Hughes, 2000).

Motility and chemotaxis of *E. coli* are among the most extensively studied biological processes (Sourjik and Wingreen, 2012; Typas and Sourjik, 2015), and the chemotaxis pathway has been used as a model to study evolutionary network optimization (Alon et al., 1999; Barkai and Leibler, 1997; Kollmann et al., 2005; Løvdok et al., 2009; Oleksiuk et al., 2011). Here, we experimentally investigated evolutionary plasticity (evolvability) of motile behavior. Experimental evolution is increasingly applied to investigate predictions of evolutionary theory, particularly in microorganisms (Barrick and Lenski, 2013; Elena and Lenski, 2003; Hindré et al., 2012; Kawecki et al., 2012; Poelwijk et al., 2011; Taute et al., 2014). For example, it has been extensively used to study the evolution of antibiotic and stress

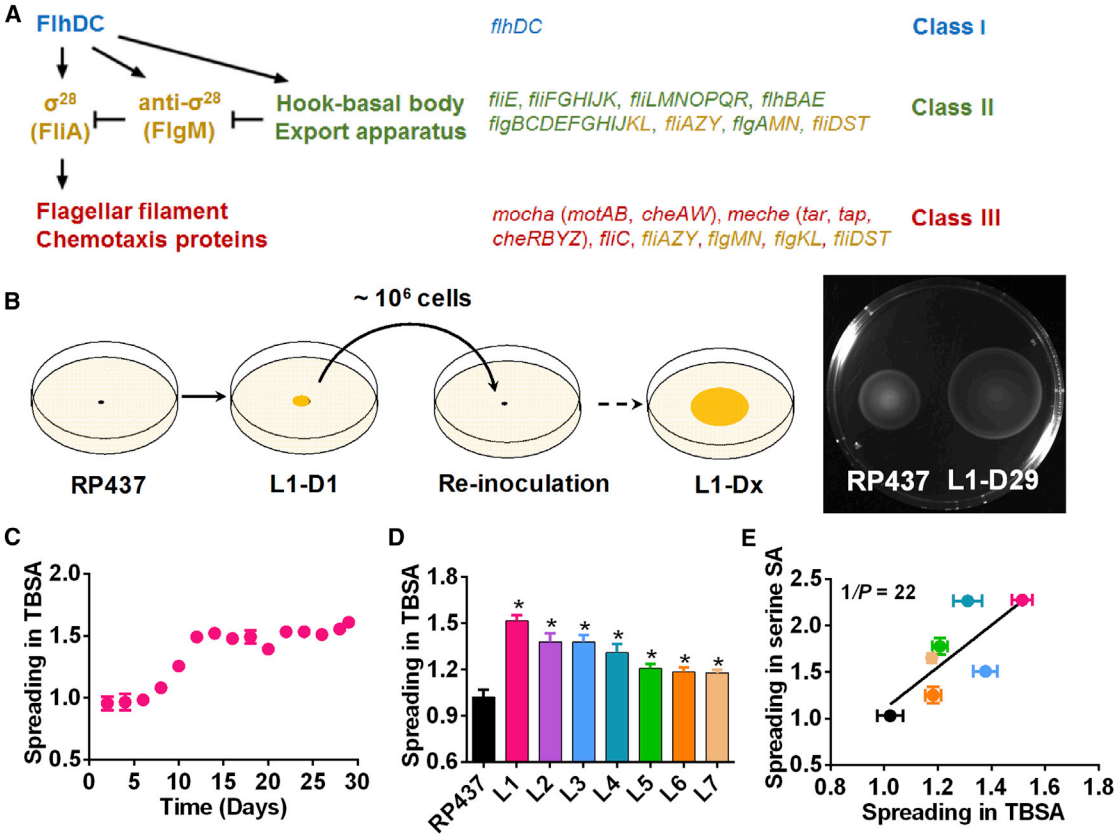

Figure 1. Experimental Evolution of Bacterial Spreading in Soft Agar

(A) Simplified schematics of the hierarchical regulatory network that controls expression of flagellar genes. Flagellar genes are organized in three classes dependent on the order of their expression, as indicated. Activity of σ^{28} (FliA) that is required for expression of class III genes (red) is controlled by a checkpoint that involves secretion of inhibitor FlgM (anti-σ^{28}) upon completion of the hook-basal body and export apparatus. Class II+III genes that have both class II and class III promoters are labeled yellow. See text for further details.

(B) Schematic illustration of the experiment. Bacteria are inoculated in the middle of the TB soft agar (TBSA) plate and allowed to spread overnight. Fastest spreaders ($\sim 10^6$ cells) are taken from the edge of spreading colony and used to inoculate a new plate. L1 indicates evolution of line 1, D1 indicates days 1 of evolution, etc. Right: spreading of the parental RP437 and evolved L1-D29 strains.

(C) Time course of enhancement of spreading during evolution of line L1, where spreading was quantified as the diameter of the colony ring on the TBSA plate and normalized to the spreading of RP437.

(D) Spreading of individually evolved lines. All lines spread significantly faster than RP437 according to a two-tailed t test (*$p < 0.05$).

(E) Correlation between spreading in TBSA and in minimal medium SA supplemented with 0.1 mM serine. Color code for individual lines here and throughout is the same as in (D). Note that because of the growth defect in minimal medium, line L2 could not be analyzed.

All data here and throughout are represented as mean ± SEM of three replicates. Correlation value is 0.76. Correlation values and p values indicated in panels were calculated as described in the Supplemental Experimental Procedures. See also Figure S1.

resistance (Chait et al., 2007; MacLean et al., 2010) or catabolism of specific nutrients (Blount et al., 2012), typically yielding mutations in a single or a small number of target genes (Blount et al., 2012; González et al., 2015; Toprak et al., 2011; Weinreich et al., 2006). Such experimental evolutionary analyses have helped to better understand several features of the evolutionary process, such as epistatic interactions between multiple mutations, evolutionary trajectories, and evolution in changing environments (Taute et al., 2014). However, understanding the evolution of complex behaviors and of the underlying regulatory networks still remains a challenge (Hindré et al., 2012).

Our results enabled us to characterize the evolvability of the regulatory network that controls bacterial motile behavior. Surprisingly, the observed evolutionary enhancement of motility was achieved through adaptive mutations in a number of functionally very different genes, encoding components of flagellar motor and export apparatus, as well as transcriptional and translational factors. Nevertheless, we showed that most of these mutations acted through a common adaptive mechanism, namely remodeling of the sigma/anti-sigma factor checkpoint, thus leading to common phenotypic changes. This remodeling of the checkpoint apparently adjusts cell motility under selection both during laboratory evolution and in natural isolates of *E. coli*. Our findings suggest that bow-tie topology can generally enhance evolvability of networks, thus indicating a previously unrecognized evolutionary function of this widespread network motif.

RESULTS

Experimental Evolution Enhances Motility and Chemotaxis

We performed experimental evolution of motile behavior of *E. coli* using selection for enhanced spreading in tryptone broth (TB) soft agar (TBSA), a porous medium containing a mixture of amino acids that act both as nutrients and as chemoattractants. Consumption of amino acids generates steep local attractant gradients that are subsequently followed by bacteria, which requires motility, chemotaxis, and growth (Berg and Turner, 1979; Wolfe and Berg, 1989). In our experiment, a cell population was allowed to spread for ~12 hr on a TBSA plate, at a growth rate of approximately one cell generation per hour, and cells from the edge of the outer spreading ring were taken to inoculate a new plate (Figure 1B). We observed that spreading of the evolved strains greatly improved within the first 5–10 rounds of selection (Figure 1C; Figure S1A), although the extent of improvement differed between independently evolved lines (L1–L7; Figure 1D). Consistently, evolved strains had a strong competitive advantage in spreading on TBSA plates compared with the parental strain RP437 (Figure S1B). Evolved *E. coli* lines showed similarly increased spreading in minimal medium soft agar (SA) supplemented with serine (Figure 1E), confirming that the observed enhancement of spreading is not specific to a particular composition of the medium.

As noted, spreading in SA that initially contains a uniform distribution of attractant requires not only motility and chemotaxis, but also consumption of attractant to create a gradient. To distinguish contributions of motility and metabolism, we tested behavior of evolved strains in gradients of a non-metabolizable analog of aspartate, α-methyl-D,L-aspartate (MeAsp), established either in SA or in liquid (Krembel et al., 2015). Evolved strains showed enhanced chemotactic spreading up the gradient in both assays (Figures S1C and S1D), confirming specific selection for improved motility and chemotaxis in our experiments.

Evolved Strains Show Changes in Motility and Flagellation

To elucidate the mechanisms that underlie the observed enhancement in motility and chemotaxis, we first examined how experimental evolution affected *E. coli* motility (Figure S2A). The most apparent phenotypic change in all evolved strains was increased swimming velocity in liquid: whereas velocity of the parental strain was comparable with that observed previously (Morehouse et al., 2005; Oleksiuk et al., 2011), it nearly doubled in some of the evolved strains. Moreover, the majority of evolved strains also exhibited an increased frequency of reorientations (tumbling rate). Both of these features were strongly correlated with spreading in TBSA, although the significance of the correlation with increased tumbling rate was weaker. As judged from the chemotactic bias, i.e., chemotactic drift normalized by the swimming velocity, higher velocity alone could mostly account for the increase in the chemotactic drift in liquid.

Our analysis further showed that evolved strains have higher frequency of flagellar motor rotation, as observed for individual motors in immobilized cells, as well as longer and, in the case of L1, also more numerous flagellar filaments (Figure S2B). The statistical analysis of these data suggest that increased flagellar length is the main determinant of higher velocity. In contrast, higher tumbling rate shows only weak correlation with increased length and number of flagella (Figure S2C). Consistent with the observed increase in flagellar length, levels of extracellular flagellin were elevated in all strains (Figure S2D).

Transcription of Class III Flagellar Genes Is Upregulated during Evolution

We next investigated whether the observed enhancement of motility may result from changes in gene expression. For that, we measured transcriptional activity at all three levels of hierarchy of flagellar genes, using reporters for representative class I (*flhD*), class II (*fliE*), and class III (*fliC*) promoters. Interestingly, we observed that the activity of P_{fliC} was upregulated in all evolved strains, whereas the activity of P_{flhD} and P_{fliE} was unchanged or even downregulated (Figure 2A). This increase in P_{fliC} activity showed strong correlation with cell spreading in TBSA (Figure 2B) and with swimming velocity (Figure 2C), indicating that specific upregulation of class III gene expression is a major determinant of the behavioral enhancement. Consistent with this assumption, an increased expression of σ^{28} (FliA) or titration of anti-σ^{28} (FlgM) from a plasmid resulted in a similar co-regulation of P_{fliC} activity with spreading in TBSA and with swimming velocity (Figures 2B and 2C). Among the other parameters, flagellar length showed highly significant correlation with P_{fliC} (and anti-correlation with P_{fliE}) activity (Figure 2D; Figure S3A), whereas flagellar number and motor speed did not show significant correlation with gene expression (Figures S3B and S3C). However, overexpression of either flagellin FliC or stator components MotA and MotB was not sufficient to increase spreading (Figure S3D), suggesting that concerted upregulation of multiple class III genes is necessary to enhance motility.

These results were further confirmed using genome-wide transcriptome profiling of the evolved strains (Figure 2E). Here, we also considered that during experimental evolution changes in gene expression could result not only from selection for enhanced motility, but also from adaptation to growth in TB at 30°C. In order to distinguish between these two types of selection, we subjected all lines to growth in liquid TB medium at 30°C for another 20 culture passages. This selection indeed either partly or entirely reversed the enhancement of spreading in TBSA (Figure S3E), and these strains were included in the transcriptome analysis.

Transcriptomics results confirmed strong correlation between enhanced spreading in soft agar and selective upregulation of class III (and class II+III) flagellar genes, consistent with higher activity of σ^{28}. Interestingly, expression of several genes related to cell wall biosynthesis (*murD*, *murE*, and *murG*) showed significant correlation with enhanced motility, whereas genes for ATP synthase (*atpA*, *atpB*, *atpC*, *atpD*, *atpE*, *atpF*, *atpG*, *atpH*, and *atpI*), amino sugar metabolism (*nanE*, *nanK*, *nagA*, *nagB*, and *nagE*), and succinyl-coenzyme A (CoA) synthetase (*sucC* and *sucD*) were weakly counter-regulated. Furthermore, a small number of genes were consistently up- or downregulated upon selection in both TBSA and liquid TB (Figure S3F), possibly associated with general growth selection.

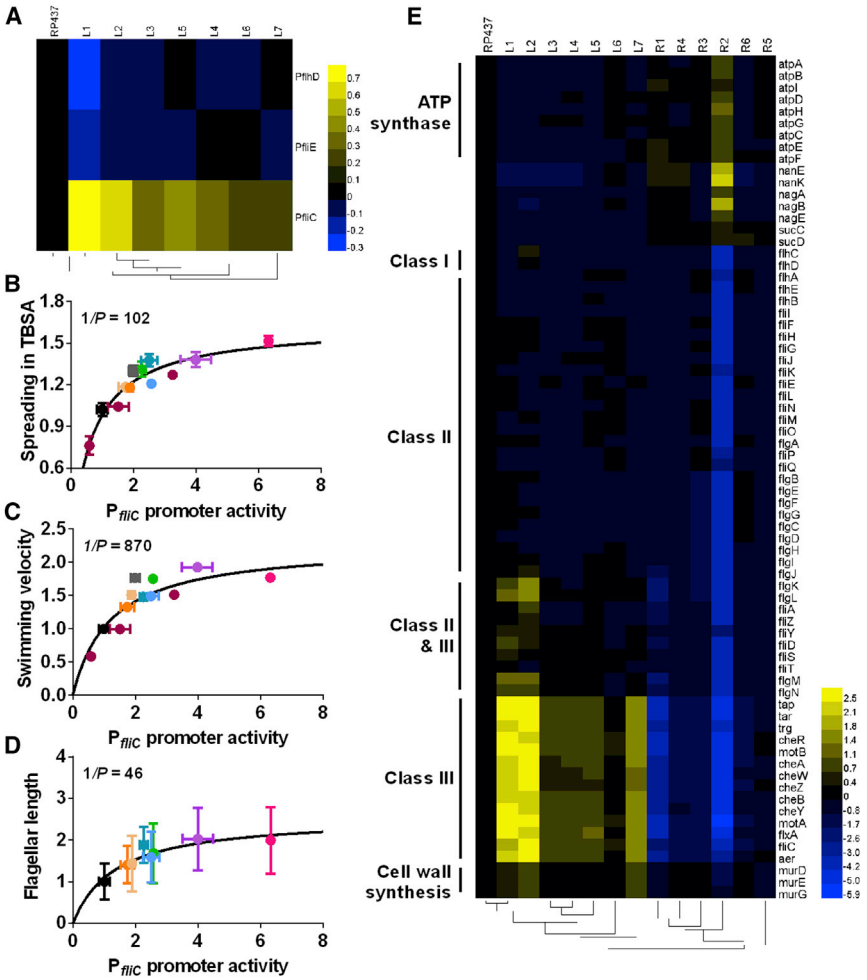

Figure 2. Upregulation of Class III Flagellar Genes during Evolution

(A) Activity of P_{flhD}, P_{fliE}, and P_{fliC} promoters in evolved strains assayed using plasmid reporters. Color code shows $\log_{10}$ of promoter activity normalized to RP437.

(B–D) Correlation between P_{fliC} promoter activity and spreading in TBSA (B), swimming velocity (C), or flagellar length (D). Gray dot indicates RP437Δ*fliA* expressing σ^{28} (FliA) from a plasmid (pBN2; no IPTG induction); dark red dots indicate RP437Δ*flgM* expressing anti-σ^{28} (FlgM) from a plasmid (pBN3; 0, 10, and 20 μM IPTG). Other dots indicate RP437 and evolved strains, with colors as in Figure 1D. Correlation values are 0.81 (B), 0.71 (C), and 0.78 (D). Lines indicate hyperbolic fits to the data for visualization.

(E) Changes in genome-wide transcription that correlate with enhanced motility, i.e., showed opposite-sign change upon selection for spreading (L1-L7) or for growth in liquid (R1-R5), as revealed by RNA-seq. Color code shows $\log_2$ of promoter activity normalized to RP437.

See also Figures S2 and S3.

Evolved Strains Carry Multiple Mutations

Subsequently, we used genome sequencing of the evolved strains to map mutations that emerged during selection for enhanced spreading in TBSA. This analysis yielded point mutations (SNPs) in 14 genes, insertions of insertion sequence 1 (IS1) transposable sequence in 5 genes, as well as 1 gene deletion (Table S1). No mutations were found in non-coding regions, including promoter sequences.

To our surprise, in spite of changes in flagellar gene expression in all evolved strains, only two of these mutations affected known transcriptional regulators of flagellar genes: one in *flgM* (anti-σ^{28}) (L3) and another in *sspA* (L1) that encodes a starvation-response factor (Hansen et al., 2005). In addition, strain L1 carries mutation in a tRNA-encoding gene *serT* that has been previously shown to affect translation of FlgM (Chevance et al., 2006). Instead, multiple mutations mapped to genes that encode functional or structural components of flagellar apparatus. Five strains (L1, L2, L4, L5, and L7) have mutations in FliI, the ATPase component of the flagellar export machinery (Fan and Macnab, 1996). Two of these strains (L1 and L4) have additional mutations in the switch components of the flagellar basal body, FliM and FliG. These proteins are required for rotation of the motor and for its control by the chemotaxis system (Bren and Eisenbach, 1998; Toker and Macnab, 1997), but they are also involved in the function of the export apparatus (González-Pedrajo et al., 2006). Furthermore, strain L3 carries, in addition to a mutation in FlgM, a mutation in CheZ, the phosphatase of the chemotaxis system, and strain L2 has an additional mutation in the aspartate chemoreceptor Tar.

A significant number of mutations mapped to genes that had no previously established relation to the flagellar regulon. These genes encoded a translation factor (*yciH*), enzymes involved in cell envelope biogenesis (*ldtB*, *mdoH*, and *idi*) or in metabolism (*hisA*, *argH*, *glpK*, and *ydfG*), transporters (*cusS* and *lacY*), and proteins of unknown function (*yebO* and *yceO*).

Multiple Adaptive Mutations Upregulate Flagellar Gene Expression and Motility

It is well established that not all mutations arising in evolutionary experiments must be adaptive (Rosenberg, 2001). To distinguish contributions of different mutations to the observed enhancement of motility, they were introduced individually into the wild-type strain and assayed for their effects on spreading in TBSA (Figure 3A). We observed that all mutations in flagellar genes, as well as in genes encoding cell envelope biogenesis enzymes, increased spreading. Moreover, spreading was also enhanced by mutations in genes encoding the transcriptional (SspA) and translational (YciH) regulators, as well as the uncharacterized protein YebO. Other mutations had little or no effect or even decreased spreading.

Despite these very different functionalities of mutated proteins, we observed that the effects of individual mutations on spreading in TBSA are highly correlated with increased

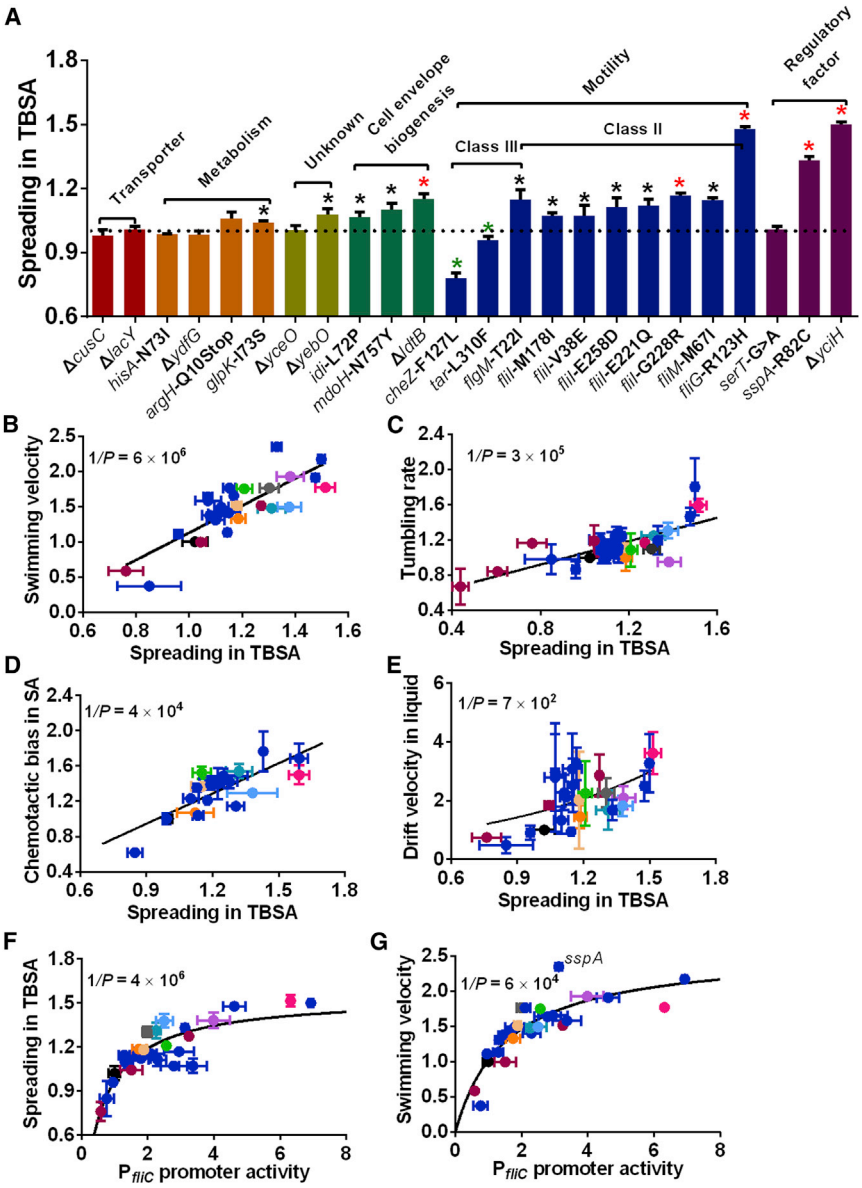

Figure 3. Upregulation of Motility and Flagellar Gene Expression by Adaptive Mutations

(A) Spreading in TBSA for RP437 strain carrying individual mutations that were identified in evolved lines. Spreading was normalized to the wild-type RP437. Significant decrease (green asterisks, $p < 0.05$ according to two-tailed t test) or increase (black asterisks, $p < 0.05$; red asterisks, $p < 0.01$) in spreading is indicated. Classification of mutated genes is indicated.

(B–E) Correlation between spreading in TBSA and swimming velocity (B), tumbling rate (C), chemotactic bias in MeAsp gradient in SA (D), or chemotactic drift velocity in MeAsp gradient in liquid (E) for strains carrying single mutations (dark blue) and for evolved strains or strains with varying levels of FliA or FlgM (colors as in Figure 2B). Data for evolved strains in (D) are taken from Figure S1C. Correlation values are 0.82 (B), 0.74 (C), 0.78 (D), and 0.59 (E). Line in (E) indicates an exponential fit.

(F and G) Correlation between P_{fliC} promoter activity and spreading in TBSA or swimming velocity for the same strains. Data for evolved strains are taken from (B) and (C). Correlation values are 0.81 (F) and 0.73 (G). Lines indicate hyperbolic fits.

See also Table S1 and Figure S4.

swimming velocity and with increased tumbling rate, and similar correlation could be observed for the evolved strains or for varying expression of σ^{28} or FlgM (Figures 3B and 3C; Figures S2A, S2B, and S4B). This confirms that increased swimming velocity and tumbling rate can account for the enhancement in spreading. Consistent with our analysis for the evolved strains, individual mutations that enhanced spreading in TBSA also conferred an advantage for following MeAsp gradients in soft agar (Figure 3D) or in liquid (Figure 3E).

Finally, essentially all individual adaptive mutations, including those in functional and structural flagellar proteins, led to elevated expression of class III genes (Figure S4A). These changes showed strong correlation with increased spreading in TBSA (Figure 3F) and with swimming velocity (Figure 3G), as observed already for the evolved strains (Figures 2B and 2C), confirming that adaptive changes in class III gene expression are the major determinant of increased motility. Interestingly, the mutation in SspA showed a disproportional enhancement of motility (Figure 3G) and not only longer, but also more numerous flagella (Figure S4C), similar to L1 that carries it.

Checkpoint Remodeling as a Mechanism of Evolutionary Plasticity

How could mutations in flagellar basal body and export apparatus mediate adaptive changes in class III gene expression? A potential mechanism linking these proteins to gene expression is secretion of the anti-σ^{28} factor FlgM. As discussed above (see Introduction and Figure 1A), FlgM-mediated inhibition ensures that σ^{28} is activated only upon assembly of the basal body that allows FlgM to be secreted. However, because FlgM is steadily expressed even after the initial checkpoint exit, its cellular levels continue to control expression of class III genes (Kollmann et al., 2005). Therefore, mutations that change the efficiency of FlgM secretion may also affect gene expression. To verify the involvement of this checkpoint control, we deleted *flgM* in all evolved strains as well as in strains that carry individual mutations. Indeed, deletion of *flgM* entirely abolished the enhancement of spreading in TBSA in three of the evolved strains (L4, L5, and L7) and reduced it in three other strains (L1, L3, and L6) (Figure 4A; Figure S5A). Similarly, in strains carrying individual mutations in flagellar genes,

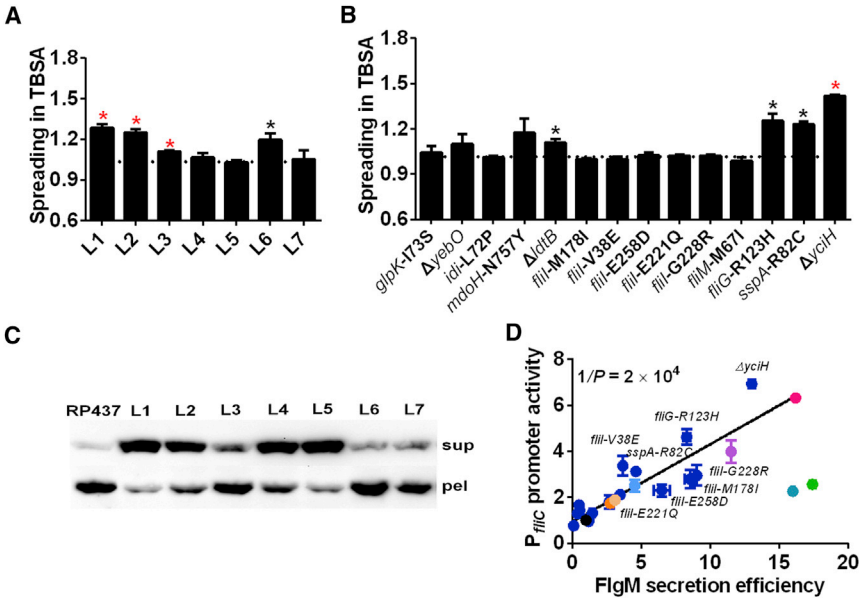

Figure 4. Sigma Factor Checkpoint Remodeling during Evolution

(A and B) Spreading in TBSA for evolved strains (A) and strains carrying individual mutations (B) upon disruption of *flgM* gene. Spreading was normalized to RP437Δ*flgM*. Black ($p < 0.05$) and red ($p < 0.01$) asterisks indicate significance of increase in spreading compared with RP437Δ*flgM*.

(C) FlgM secretion efficiency in indicated strains, assayed by measuring levels of FlgM-HA in supernatant (sup) and pellet (pel) fractions.

(D) Correlation between FlgM secretion efficiency and P_{fliC} promoter activity. Individual mutations that result in highest increase in secretion are indicated. Correlation value is 0.72. Color code is as in Figure 3.

See also Figure S5.

spreading enhancement was either abolished (for *fliI* or *fliM* mutations) or reduced (for *fliG* mutation) by the deletion of *flgM* (Figure 4B; Figure S5B). This confirms our hypothesis that increased secretion of the anti-σ^{28} factor FlgM is the main mechanism of adaptive motility enhancement via mutations in flagellar proteins.

Interestingly, deletion of *flgM* also reduced the effects of the *sspA* and *yciH* mutations, although these gene products have no established connection to the regulation of FlgM secretion. Nevertheless, the effects of *yciH*, *ldtB*, *mdoH*, *yebO*, and *sspA* mutations on motility appear to be at least partly independent of the FlgM secretion, which may explain (residual) FlgM-independent enhancement of spreading that is observed in strains L1, L2, L3, and L6 that carry these mutations.

In order to directly confirm the connection between the checkpoint remodeling and enhanced expression of class III genes, we quantified efficiency of FlgM secretion. Consistent with our explanation, in all evolved strains FlgM secretion efficiency was significantly enhanced, leading to a lower cellular level of FlgM relative to its level in the supernatant (Figure 4C). Moreover, there was a strong correlation between the FlgM secretion efficiency and the level of class III gene expression, both in the evolved strains and in strains containing individual mutations that enhanced motility (Figure 4D). Such correlation was not observed for secretion efficiency of FliC (Figure S5C), suggesting that the adaptive enhancement of secretion is specific to FlgM.

Trade-Off between Motility and Growth Fitness

It is well established that evolution frequently needs to optimize different conflicting functions, thus leading to adaptive trade-offs (Schuetz et al., 2012; Shoval et al., 2012). For expression of highly abundant flagellar and chemotaxis proteins, the most likely fitness trade-off may be associated with growth. Indeed, when relative growth fitness of the evolved strains in liquid TB was plotted as a function of P_{fliC} promoter activity, clear anticorrelation between the two was observed (Figure 5A). A similarly apparent trade-off could be observed between the growth fitness and swimming velocity (Figure 5B). Consistent with that, growth rate increased upon disruption of *flhC* (eliminating expression of the entire flagellar regulon) or *fliA* (eliminating expression of class III genes), and it was severely reduced by deletion of *flgM* (upregulation of class III genes). Disruption of *fliC* gene increased growth rate nearly as much as *fliA* deletion, confirming that a large part of fitness cost associated with class III gene expression is due to production of flagellin. Indeed, deletion of *fliC* largely alleviated the fitness burden in strain L1 (Figure 5C). The remaining cost might arise from expression of other class III genes or from the energy expenditure for flagellar rotation. However, mutations in *sspA* and *yciH* seem to generally incur disproportionally high cost compared with their fitness increase, likely because they affect not only motility, but also other cellular functions.

Checkpoint Activity Correlates with Motility of Natural *E. coli* Isolates

We hypothesized that the observed mechanism of motility enhancement might also play a role in the evolutionary plasticity of natural isolates of *E. coli*. Consistent with that, we observed a highly significant correlation between activity of P_{fliC} promoter and spreading of motile natural isolates that were randomly selected from the ECOR collection (Ochman and Selander, 1984) (Figure 6A). In contrast, correlation with the activity of P_{fliE} or P_{flhD} promoters was either much weaker or non-significant (Figures 6B–6D). This confirms our hypothesis that variation in motility of the natural isolates is mainly determined by expression of class III genes rather than of the entire flagellar regulon. The underlying cause again appears to be the plasticity of checkpoint efficiency, because secretion of FlgM is highly correlated with the spreading in TBSA and with the P_{fliC} activity in most natural isolates (Figures 6E and 6F).

Bow-Tie Topology Accelerates Network Evolution

Taken together, our findings demonstrate that mutations in multiple flagellar proteins modulate motility through a common

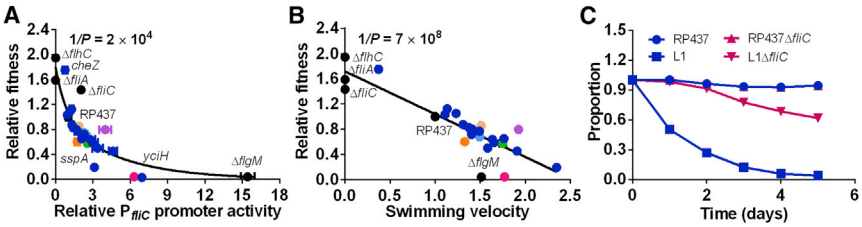

Figure 5. Trade-Off between Motility and Fitness

(A and B) Correlation between relative growth fitness and P_{fliC} promoter activity (A) or swimming velocity (B). Relative growth was determined by co-incubation of tested strain with the wild-type (RP437), and relative fitness was defined as the fraction of the tested strain after 5-day incubation normalized by the fraction at inoculation (0.5). Correlation values are −0.68 (A) and −0.88 (B). Line in (A) indicates a bi-exponential decay fit. Color code is as in Figure 3.

(C) Proportions of indicated strains in competition assay over time.

control of FlgM secretion (Figure 7A). We also obtained similar mutations in flagellar genes in another evolutionary experiment, where selection for motility was performed on minimal medium SA plates (Table S2). We thus hypothesized that the multi-input motif present in the flagellar checkpoint control, but also common in many other cellular networks, might play a general role in evolution. To test this hypothesis, we simulated in silico evolution of a simple bow-tie network where multiple input nodes (X1 to X3) affect activity of a common intermediate node (Y) that in turn activates the output node (Z), and compared it with evolution of linear networks where either one or multiple input nodes act independently (Figure 7B). In these simulations, the fitness increase for the bow-tie network under selection was markedly faster than for the linear networks (Figure 7C), even though the multi-input linear network can in principle attain the same maximal fitness as the bow-tie network (see Supplemental Experimental Procedures). Our analysis thus confirms that the bow-tie topology can accelerate network evolution.

DISCUSSION

It is commonly assumed that as a consequence of long-term selection, living organisms have evolved to perform different tasks optimally (de Vos et al., 2013; Flamholz et al., 2013; Ibarra et al., 2002; Kollmann et al., 2005; Noor et al., 2010; Notebaart et al., 2014; Schuetz et al., 2012; Zarrinpar et al., 2003). However, proving this assumption is difficult, not least because details of the past evolutionary selection pressure and the underlying trade-offs between different functions are typically unknown (Hindré et al., 2012). Moreover, establishing the genotype-to-phenotype mapping during evolutionary adaptation remains a challenge, given the difficulty in distinguishing between neutral and adaptive mutations and specifically linking a mutation to one and unlinking it from other traits (Lehner, 2013). Although experimental evolution can address some of these questions by subjecting (micro-)organisms to selection under defined laboratory conditions and monitoring ensuing changes in their phenotype and genotype (Hindré et al., 2012), it is most frequently applied to simple traits that involve only one or a few proteins (Blount et al., 2012; González et al., 2015; Toprak et al., 2011; Weinreich et al., 2006). Here, we used selection for *E. coli* motility in a porous environment to investigate how adaptive evolution under a specific selection pressure shapes this complex bacterial phenotype and what are the internal constraints and underlying mechanisms of genotype and phenotype remodeling.

We observed that enhanced motility evolved in all our experiments, consistent with high selective pressure at the edge of the spreading colony caused by nutrient depletion. On the phenotypic level, the enhancement of *E. coli* motility in soft agar was primarily driven by increased swimming velocity, but also by increased tumbling rate. This phenotypic adaptation can be well understood in the context of bacterial chemotaxis between traps created by agar (Wolfe and Berg, 1989). Here, similar to the chemotaxis in liquid, bacteria must swim up the gradient to detect changes in chemical concentration and to bias their motility by reducing tumbling rate (Sourjik and Wingreen, 2012). Higher swimming velocity should thus generally enhance spreading by accelerating both the random movement and chemotaxis. However, in the porous environment, higher swimming velocity alone would also lead to more frequent trapping of bacteria in the agar pores, which would limit spreading. The observed increase in tumbling rate may alleviate this hindrance by enabling bacteria not only to cover distances between pores faster, but also to escape them more efficiently (Wolfe and Berg, 1989).

On the molecular level, this phenotypic adaptation could be accounted for by upregulated expression of class III flagellar genes. This upregulation led to increased flagellar length and motor rotation rate, whereby the former was apparently the main determinant of faster swimming. Such specific upregulation of class III genes in all of the independent evolutionary experiments was surprising, because the established transcriptional regulation of flagellar genes in *E. coli* occurs primarily at the upper (class I) level of the regulatory hierarchy and affects expression of all three gene classes (Fahrner and Berg, 2015) (Figure 7A). Moreover, this is seemingly in contrast to previous studies showing that poorly motile *E. coli* strains could activate motility through insertion of insertion sequence 5 (IS*5*) element into the regulatory region of the *flhDC* operon (Barker et al., 2004; Wang and Wood, 2011). On the other hand, we observed no transcriptional regulation of individual class III genes or changes in the network topology. Our results thus demonstrate that concerted upregulation of multiple class III genes is required, and also sufficient, to enhance motility, likely because not only FliC, but also other products of class III (and class II+III) genes are required for assembly and energizing of longer flagella, and thereby for faster swimming. Consistent with that explanation, proton channel components MotA and MotB, as well as chaperones (e.g., FliS) that are required for FliC filament assembly (Auvray et al., 2001), are encoded by class III or class

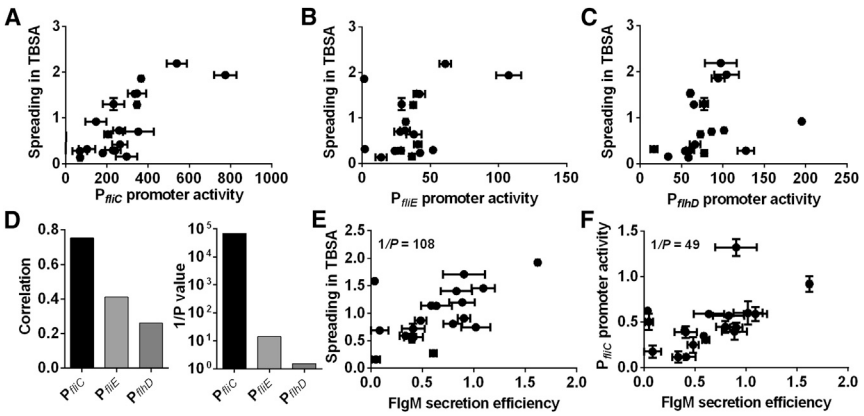

Figure 6. Correlation between Flagellar Gene Expression and Motility in Natural Isolates

(A–D) Spreading in TBSA as a function of P_{fliC} (A), P_{fliE} (B), or P_{flhD} (C) promoter activity in natural *E. coli* isolates, and significance of correlation based on regression analysis of these data (D).

(E and F) Spreading in TBSA (E) and P_{fliC} promoter activity (F) as a function of FlgM secretion efficiency.

II+III genes. We therefore propose that, besides its importance for sequential ordering of expression (Chilcott and Hughes, 2000; Kalir et al., 2001), the topology of flagellar gene regulation may be a consequence of evolutionary selection for high plasticity of flagellar motility. This way, all class III genes that are required for increased motility are under common regulatory control, which enables concerted evolutionary tuning of their levels.

Similarly unexpectedly, we observed that the main mechanism of the adaptive upregulation of class III genes relies on enhanced secretion of the anti-sigma factor FlgM rather than on other possible mechanisms, such as upregulation of the expression or activity of σ^{28}. The role of FlgM secretion as a checkpoint control for the intermediate stage of flagella assembly in *E. coli* and other bacteria is well established. The observed recurrent utilization of this checkpoint in evolutionary enhancement of cell motility suggests that it also serves another, entirely different adaptive function, namely in enabling bacteria to efficiently adjust motility dependent on environmental selection. This adjustment occurs through modulation of FlgM secretion, and it can be mediated by mutations in a number of proteins that form flagellar secretion machinery or regulate secretion in other ways (Figure 7A). Consistent with its general function in evolutionary plasticity, the σ^{28}/FlgM checkpoint remodeling appears to explain the tuning of motility not only under laboratory selection, but also in natural isolates of *E. coli*. Interestingly, although the exact mechanisms through which mutations in different motor proteins enhance secretion remain to be investigated, our analysis suggests that this enhancement is specific to FlgM as a substrate. Future studies of these mutations might thus provide further insights into specificity and evolution of the export machinery of type III secretion systems.

We believe that the observed adaptive mechanism may be indicative of a previously unrecognized general role of global checkpoint control mechanisms, and of bacterial sigma/anti-sigma factors in particular, in the evolutionary plasticity of gene expression. Most such global control networks possess a specific bow-tie structure, where multiple regulatory inputs control the activity (or levels) of a key factor that in turn regulates multiple downstream targets, e.g., expression of different genes. Previous adaptive explanations for such network structure suggested that it might enable independent evolution of the input and output functions without affecting the regulatory core (Csete and Doyle, 2004) and also compress cellular input information (Friedlander et al., 2015). Our results strongly suggest that such multi-input design also enhances evolutionary plasticity of the regulatory networks, by substantially increasing the number of possible mutations that affect activity of the common central process (the σ^{28}/FlgM checkpoint in our case), and therefore adjust regulation of the downstream targets. Although it is difficult to assess the relative importance of selection for these individual properties, the enhanced evolvability is likely to be a major factor in the overall evolutionary enrichment of the bow-tie motifs in cellular networks.

Why did phenotype remodeling not occur at the level of class I gene expression, which is controlled by multiple transcriptional inputs (Figure 7C)? For one, the transcription factors involved are not unique to the flagellar regulon, meaning that changes in their activity are likely to affect other cellular functions. Moreover, instead of increasing flagellar length, the upregulation of the entire flagellar regulon might increase flagellar number, which was apparently less critical for the enhancement of motility in our experiments. We thus hypothesize that although previously reported activation of the *flhDC* operon by IS*5* insertion (Barker et al., 2004; Wang and Wood, 2011) can naturally act as a binary ON-switch of motility, subsequent gradual tuning of motility under selection is more efficiently achieved through specific class III gene upregulation. Further supporting the adaptive advantage of such regulation, we observed that even mutations resulting in the FlgM-independent enhancement of motility led to higher expression of class III, but not of other flagellar genes.

Finally, we observed that selection for increased motility carries a cost of reduced growth fitness, meaning that evolution cannot simultaneously maximize both functions. Such conflict between optimization objectives is common in evolution (Garland, 2014; Roff and Fairbairn, 2007), and it might explain why many laboratory *E. coli* strains, as well as natural isolates, have attenuated motility. Interestingly, recent theoretical analysis has shown that for multiple conflicting optimization tasks, the existing phenotypes fall on a specific Pareto optimality front connecting both extremes of optimization, which in case of two tasks is a line (Shoval et al., 2012). In apparent agreement with this prediction, all strains in our analysis mapped roughly along the same line when growth fitness was plotted against swimming velocity. This was even true for strains that carry individual mutations, which is not trivial because of possible epistatic interactions between multiple mutations in evolved strains. We believe

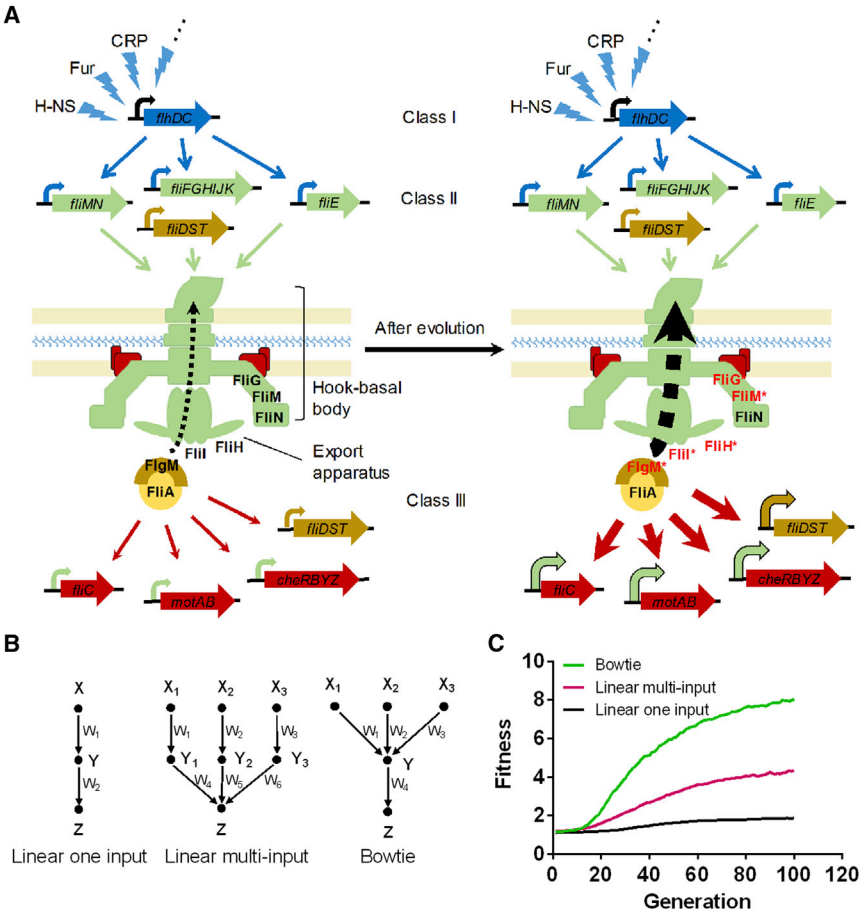

Figure 7. Multi-input Checkpoint Control Mediates Evolution of Motility

(A) Remodeling of flagellar checkpoint control under selection. Left: flagellar genes are organized in three classes (see Figure 1 and text for details). Checkpoint control couples expression of class III genes (red/orange) to completion of flagellar hook-basal body (HBB) through secretion of FlgM that releases σ^{28} (FliA). Class I genes (blue) are controlled by a number of upstream transcriptional regulators, only some of which are shown. Right: adaptive mutations in multiple HBB (FliM and FliG) or export apparatus (FliI and FliH) proteins encoded by class II genes (green) enhance export efficiency of FlgM, thereby increasing cellular levels of active FliA and leading to upregulation of class III genes. See also Table S2.

(B and C) In silico evolution of linear and bow-tie networks. Networks have either one (X) or multiple (X_1 to X_3) inputs that activate the output (Z) through independent or common intermediates (Y), as schematically shown (B). The strength of activation is denoted by W. Networks were subject to simulated evolution as described in the Supplemental Experimental Procedures for 100 generations. Median fitness, assumed to be proportional to Z, was calculated for simulations of each network with 100 randomly selected initial parameter sets (C) and plotted against the number of generations.

that such universal alignment points to remodeling of FlgM secretion as a general mechanism for optimal tuning of the motility-growth trade-off, so that any change in FlgM export would move the phenotype along the same Pareto optimization line.

In conclusion, experimental evolution demonstrated that bacteria can rapidly adjust such a complex trait as motility under selection pressure, following a defined trade-off line with conflicting optimization for growth. This high phenotypic plasticity appears to be inherent in the design of the hierarchical flagellar gene regulatory network, where genes modulating motility and chemotaxis are under the common control of a sigma/anti-sigma factor checkpoint that can be rapidly tuned under selection. Thus, besides its well-established function in the control of timing of flagellar gene expression, this checkpoint plays a key role in the evolutionary plasticity of *E. coli* motility. This latter function seems to be aided by its bow-tie architecture, and we propose that the similar design of other global regulatory networks might generally promote evolutionary adaptation.

EXPERIMENTAL PROCEDURES

Strains and Plasmids

All strains used in this study were derived from *E. coli* K12 strain RP437 that is commonly used as a wild-type for chemotaxis and motility studies (Parkinson, 1978) and has constitutively activated motility because of IS*5* insertion in the promoter region of *flhDC* operon (Barker et al., 2004). Details of strain and plasmid construction can be found in the Supplemental Experimental Procedures. Cells were grown at 30°C in TB medium [1% tryptone and 0.5% sodium chloride (NaCl)] supplemented with appropriate antibiotics (ampicillin: 100 $\mu g \cdot mL^{-1}$, kanamycin: 50 $\mu g \cdot mL^{-1}$).

Experimental Microevolution

Microevolution of *E. coli* strain RP437 was performed in 0.3% soft agar plates supplemented with TB. After an overnight incubation at 30°C, cells from the edge of the spreading ring were collected and re-inoculated onto a new soft agar plate. The same procedure was repeated 20–30 times, as indicated. For reverse evolution, evolved strains were repeatedly grown overnight in 3 mL liquid TB at 30°C.

Motility Analyses

For motility analysis, *E. coli* cells were grown in 10 mL TB medium at 34°C in a rotary shaker at 180 rpm. Cells (1 mL) at mid-log phase (OD_{600} [optical density at 600 nm] = 0.6) were collected and re-suspended in 1 mL tethering buffer (10 mM K_2HPO_4, 10 mM KH_2PO_4, 100 μM EDTA, 1 μM L-methionine, 10 mM lactic acid [pH 7.0]). Bacterial spreading was measured by inoculating 2 μL cell suspension at the top of 0.3% soft agar containing either TB or Minimal A medium supplemented with 0.1 mM aspartate or serine as indicated, after 7–8 hr incubation in TB or 20–22 hr incubation in Minimal A soft agar at 30°C. For measurements of chemotactic bias in soft agar, gradient of MeAsp was established in Minimal A soft agar containing glucose for 14 hr at 4°C before cell inoculation as described previously (Krembel et al., 2015). Swimming velocity and tumbling rate were measured by cell tracking in a glass chamber using phase-contrast microscopy (Nikon TI Eclipse, 10× objective, NA = 0.3, CMOS camera EoSens 4CXP). Drift velocity and chemotaxis efficiency in MeAsp gradient were tested in a microchamber made of poly-dimethylsiloxane (PDMS) using differential dynamic microscopy (DDM) (Wilson

et al., 2011) and phase differential microscopy (φDM) (Colin et al., 2014). The cells were subjected to a linear gradient of MeAsp of 100 μM per 2 mm, and average concentration at the measurement segment was 50 μM. All data were analyzed using ImageJ (https://imagej.nih.gov/ij/) with custom-written plugins for swimming velocity, drift velocity, and tumbling rate analysis (Colin et al., 2014).

Genome and Transcriptome Analyses

E. coli cells were grown in TB as described above and harvested at mid-log phase (OD_{600} = 0.6). DNA samples were prepared using commercial kits (QIAGEN), and RNA samples were prepared using hot acid/phenol RNA extraction method (Maniatis et al., 1982). Genome sequencing was performed at GATC Biotech; RNA sequencing was performed at the BioQuant sequencing facility (University of Heidelberg). All sequencing data were analyzed using DNASTAR Lasergene software with *E. coli* strain MG1655 as reference template.

Promoter Activity Analysis

For promoter activity assays, *E. coli* strains transformed with reporter plasmids were grown in TB supplemented with kanamycin in 96-well plates at 30°C in a rotary shaker at 180 rpm. Cell fluorescence was measured using flow cytometry on BD LSRFortessa SORP cell analyzer (BD Biosciences).

Growth Fitness Analysis

For growth fitness measurements, equal amounts of a tested strain expressing CFP (pVS129) and the wild-type RP437 strain labeled with yellow fluorescent protein (YFP) (pVS132) were inoculated into 1 mL of TB medium supplemented with ampicillin and 20 μM isopropyl-β-D-thiogalactopyranosid (IPTG). After growth in a shaker at 30°C for 20 hr, 10 μL of cell suspensions was transferred into 1 mL PBS (pH 7.4), and the numbers of CFP- and YFP-labeled cells were measured by flow cytometry as described above. The culture was then reinoculated and the dynamics of the two cell populations was so monitored for 5 days.

Secretion Assay

Protein secretion was assayed using C-terminal fusions of a hemagglutinin (HA) tag to FlgM or to 175-amino-acid N-terminal fragment of FliC. The latter construct additionally contained a 71-bp 5′ untranslated region upstream of *fliC.* Cells were grown in TB as described above. FlgM-HA expression from a plasmid pBN4 was induced by 100 μM IPTG; $FliC^{1-175}$-HA expression from a plasmid pBN5 was induced by 50 μM IPTG. Protein levels in the pellet and supernatant, respectively, were analyzed by immunoblotting as described in the Supplemental Experimental Procedures.

Quantification of Extracellular and Intracellular Flagellin

For measurements of FliC levels, density of cell culture was adjusted to OD_{600} = 1, and extracellular FliC filaments were sheared by Precellys homogenizer (Bertin Technologies) at 4,500 rpm for 20 s. Afterward, bacterial cells were collected by centrifugation (13,000 rpm for 1 min) at 4°C. Supernatants and pellets were collected separately for SDS-PAGE and immunoblotting. Anti-FliC antibody at a 1:10,000 dilution and secondary anti-rabbit IgG antibody labeled with peroxidase at a 1:5,000 dilution were used for detection.

Motor Rotation Assay

Motor rotation assay was conducted as described previously (Ryu et al., 2000) with minor modifications. Cells grown in TB medium were collected, re-suspended in tethering buffer, and flagella were sheared by 60 passages through 26 G syringe needle. Cells were allowed to settle on glass coverslips treated with poly-L-lysine (Sigma) and incubated for 5 min with a suspension of 1.1 μm polystyrene beads (Sigma). Unattached beads were washed away using tethering buffer supplemented with 20% TB. Rotation of beads was monitored using phase-contrast microscopy (40× magnification) at 1,000 Hz for 20 s. The beads were tracked using ImageJ with a custom-written plugin, and the traces were analyzed using MATLAB to extract the frequency of rotation.

Electron Microscopy

Carbon-coated copper grids (400 mesh) were hydrophilized by glow discharging (PELCO easiGlow; Ted Pella). Five microliters of a cell suspension (grown to OD_{600} = 0.5–0.6 as described above) was applied onto the hydrophilized grids and stained with 2% uranyl acetate after a short washing step with water. Samples were analyzed using a JEOL JEM-2100 transmission electron microscope with an acceleration voltage of either 80 or 200 kV. F214 FastScan CCD camera (TVIPS; Gauting) was used for image acquisition.

Statistical Analysis and Simulations

Details of statistical data analysis and computational simulations are described in the Supplemental Experimental Procedures.

ACCESSION NUMBERS

The accession number for the original sequencing data reported in this paper is NIH SRA: SRP095233.

SUPPLEMENTAL INFORMATION

Supplemental Information includes Supplemental Experimental Procedures, five figures, and two tables and can be found with this article online at http://dx.doi.org/10.1016/j.celrep.2016.12.088.

AUTHOR CONTRIBUTIONS

V.S., B.N., and F.S.P. designed experiments. B.N., F.S.P., R.C., and T.H. performed experiments. B.N., B.G., and R.C. analyzed data. B.G. performed computer simulations. V.S. and B.N. wrote the manuscript.

ACKNOWLEDGMENTS

We thank Howard C. Berg, Ned S. Wingreen, Sean Murray, and Kelly Hughes for insightful discussions and comments on the manuscript; Lars Velten for help with experiments; and Karen A. Fahrner for providing pKAF131. This work was supported by grant 294761-MicRobE from the European Research Council and grant R01 GM082938 from the NIH.

Received: September 16, 2016
Revised: November 16, 2016
Accepted: December 27, 2016
Published: January 24, 2017

REFERENCES

Aldridge, P., and Hughes, K.T. (2002). Regulation of flagellar assembly. Curr. Opin. Microbiol. *5*, 160–165.

Alon, U., Surette, M.G., Barkai, N., and Leibler, S. (1999). Robustness in bacterial chemotaxis. Nature *397*, 168–171.

Auvray, F., Thomas, J., Fraser, G.M., and Hughes, C. (2001). Flagellin polymerisation control by a cytosolic export chaperone. J. Mol. Biol. *308*, 221–229.

Barkai, N., and Leibler, S. (1997). Robustness in simple biochemical networks. Nature *387*, 913–917.

Barker, C.S., Prüss, B.M., and Matsumura, P. (2004). Increased motility of *Escherichia coli* by insertion sequence element integration into the regulatory region of the *flhD* operon. J. Bacteriol. *186*, 7529–7537.

Barrick, J.E., and Lenski, R.E. (2013). Genome dynamics during experimental evolution. Nat. Rev. Genet. *14*, 827–839.

Berg, H.C., and Turner, L. (1979). Movement of microorganisms in viscous environments. Nature *278*, 349–351.

Blount, Z.D., Barrick, J.E., Davidson, C.J., and Lenski, R.E. (2012). Genomic analysis of a key innovation in an experimental *Escherichia coli* population. Nature *489*, 513–518.

Bren, A., and Eisenbach, M. (1998). The N terminus of the flagellar switch protein, FliM, is the binding domain for the chemotactic response regulator, CheY. J. Mol. Biol. *278*, 507–514.

Chait, R., Craney, A., and Kishony, R. (2007). Antibiotic interactions that select against resistance. Nature *446*, 668–671.

Chevance, F.F.V., and Hughes, K.T. (2008). Coordinating assembly of a bacterial macromolecular machine. Nat. Rev. Microbiol. *6*, 455–465.

Chevance, F.F., Karlinsey, J.E., Wozniak, C.E., and Hughes, K.T. (2006). A little gene with big effects: a *serT* mutant is defective in *flgM* gene translation. J. Bacteriol. *188*, 297–304.

Chilcott, G.S., and Hughes, K.T. (2000). Coupling of flagellar gene expression to flagellar assembly in *Salmonella enterica* serovar typhimurium and *Escherichia coli*. Microbiol. Mol. Biol. Rev. *64*, 694–708.

Colin, R., Zhang, R., and Wilson, L.G. (2014). Fast, high-throughput measurement of collective behaviour in a bacterial population. J. R. Soc. Interface *11*, 20140486.

Csete, M., and Doyle, J. (2004). Bow ties, metabolism and disease. Trends Biotechnol. *22*, 446–450.

de Vos, M.G.J., Poelwijk, F.J., and Tans, S.J. (2013). Optimality in evolution: new insights from synthetic biology. Curr. Opin. Biotechnol. *24*, 797–802.

Elena, S.F., and Lenski, R.E. (2003). Evolution experiments with microorganisms: the dynamics and genetic bases of adaptation. Nat. Rev. Genet. *4*, 457–469.

Fahrner, K.A., and Berg, H.C. (2015). Mutations that stimulate *flhDC* expression in *Escherichia coli* K-12. J. Bacteriol. *197*, 3087–3096.

Fan, F., and Macnab, R.M. (1996). Enzymatic characterization of FliI. An ATPase involved in flagellar assembly in *Salmonella typhimurium*. J. Biol. Chem. *271*, 31981–31988.

Flamholz, A., Noor, E., Bar-Even, A., Liebermeister, W., and Milo, R. (2013). Glycolytic strategy as a tradeoff between energy yield and protein cost. Proc. Natl. Acad. Sci. USA *110*, 10039–10044.

Friedlander, T., Mayo, A.E., Tlusty, T., and Alon, U. (2015). Evolution of bow-tie architectures in biology. PLoS Comput. Biol. *11*, e1004055.

Garland, T., Jr. (2014). Trade-offs. Curr. Biol. *24*, R60–R61.

González, C., Ray, J.C.J., Manhart, M., Adams, R.M., Nevozhay, D., Morozov, A.V., and Balázsi, G. (2015). Stress-response balance drives the evolution of a network module and its host genome. Mol. Syst. Biol. *11*, 827.

González-Pedrajo, B., Minamino, T., Kihara, M., and Namba, K. (2006). Interactions between C ring proteins and export apparatus components: a possible mechanism for facilitating type III protein export. Mol. Microbiol. *60*, 984–998.

Hansen, A.M., Qiu, Y., Yeh, N., Blattner, F.R., Durfee, T., and Jin, D.J. (2005). SspA is required for acid resistance in stationary phase by downregulation of H-NS in *Escherichia coli*. Mol. Microbiol. *56*, 719–734.

Hengge, R. (2009). Proteolysis of sigmaS (RpoS) and the general stress response in *Escherichia coli*. Res. Microbiol. *160*, 667–676.

Hindré, T., Knibbe, C., Beslon, G., and Schneider, D. (2012). New insights into bacterial adaptation through in vivo and in *silico* experimental evolution. Nat. Rev. Microbiol. *10*, 352–365.

Hughes, K.T., Gillen, K.L., Semon, M.J., and Karlinsey, J.E. (1993). Sensing structural intermediates in bacterial flagellar assembly by export of a negative regulator. Science *262*, 1277–1280.

Ibarra, R.U., Edwards, J.S., and Palsson, B.O. (2002). *Escherichia coli* K-12 undergoes adaptive evolution to achieve in *silico* predicted optimal growth. Nature *420*, 186–189.

Kalir, S., McClure, J., Pabbaraju, K., Southward, C., Ronen, M., Leibler, S., Surette, M.G., and Alon, U. (2001). Ordering genes in a flagella pathway by analysis of expression kinetics from living bacteria. Science *292*, 2080–2083.

Kawecki, T.J., Lenski, R.E., Ebert, D., Hollis, B., Olivieri, I., and Whitlock, M.C. (2012). Experimental evolution. Trends Ecol. Evol. *27*, 547–560.

Kollmann, M., Løvdok, L., Bartholomé, K., Timmer, J., and Sourjik, V. (2005). Design principles of a bacterial signalling network. Nature *438*, 504–507.

Krembel, A., Colin, R., and Sourjik, V. (2015). Importance of multiple methylation sites in *Escherichia coli* chemotaxis. PLoS ONE *10*, e0145582.

Lehner, B. (2013). Genotype to phenotype: lessons from model organisms for human genetics. Nat. Rev. Genet. *14*, 168–178.

Løvdok, L., Bentele, K., Vladimirov, N., Müller, A., Pop, F.S., Lebiedz, D., Kollmann, M., and Sourjik, V. (2009). Role of translational coupling in robustness of bacterial chemotaxis pathway. PLoS Biol. *7*, e1000171.

MacLean, R.C., Hall, A.R., Perron, G.G., and Buckling, A. (2010). The population genetics of antibiotic resistance: integrating molecular mechanisms and treatment contexts. Nat. Rev. Genet. *11*, 405–414.

Maniatis, T., Fritsch, E.F., and Sambrook, J. (1982). Molecular Cloning: A Laboratory Manual (Cold Spring Harbor Laboratory).

Minamino, T., and Imada, K. (2015). The bacterial flagellar motor and its structural diversity. Trends Microbiol. *23*, 267–274.

Morehouse, K.A., Goodfellow, I.G., and Sockett, R.E. (2005). A chimeric N-terminal *Escherichia coli*–C-terminal *Rhodobacter sphaeroides* FliG rotor protein supports bidirectional *E. coli* flagellar rotation and chemotaxis. J. Bacteriol. *187*, 1695–1701.

Mukherjee, S., and Kearns, D.B. (2014). The structure and regulation of flagella in *Bacillus subtilis*. Annu. Rev. Genet. *48*, 319–340.

Noor, E., Eden, E., Milo, R., and Alon, U. (2010). Central carbon metabolism as a minimal biochemical walk between precursors for biomass and energy. Mol. Cell *39*, 809–820.

Notebaart, R.A., Szappanos, B., Kintses, B., Pál, F., Györkei, Á., Bogos, B., Lázár, V., Spohn, R., Csörgő, B., Wagner, A., et al. (2014). Network-level architecture and the evolutionary potential of underground metabolism. Proc. Natl. Acad. Sci. USA *111*, 11762–11767.

Ochman, H., and Selander, R.K. (1984). Standard reference strains of *Escherichia coli* from natural populations. J. Bacteriol. *157*, 690–693.

Oleksiuk, O., Jakovljevic, V., Vladimirov, N., Carvalho, R., Paster, E., Ryu, W.S., Meir, Y., Wingreen, N.S., Kollmann, M., and Sourjik, V. (2011). Thermal robustness of signaling in bacterial chemotaxis. Cell *145*, 312–321.

Österberg, S., del Peso-Santos, T., and Shingler, V. (2011). Regulation of alternative sigma factor use. Annu. Rev. Microbiol. *65*, 37–55.

Paget, M.S. (2015). Bacterial sigma factors and anti-sigma factors: structure, function and distribution. Biomolecules *5*, 1245–1265.

Parkinson, J.S. (1978). Complementation analysis and deletion mapping of *Escherichia coli* mutants defective in chemotaxis. J. Bacteriol. *135*, 45–53.

Poelwijk, F.J., de Vos, M.G.J., and Tans, S.J. (2011). Tradeoffs and optimality in the evolution of gene regulation. Cell *146*, 462–470.

Roff, D.A., and Fairbairn, D.J. (2007). The evolution of trade-offs: where are we? J. Evol. Biol. *20*, 433–447.

Rosenberg, S.M. (2001). Evolving responsively: adaptive mutation. Nat. Rev. Genet. *2*, 504–515.

Rudner, D.Z., and Losick, R. (2001). Morphological coupling in development: lessons from prokaryotes. Dev. Cell *1*, 733–742.

Ryu, W.S., Berry, R.M., and Berg, H.C. (2000). Torque-generating units of the flagellar motor of *Escherichia coli* have a high duty ratio. Nature *403*, 444–447.

Schuetz, R., Zamboni, N., Zampieri, M., Heinemann, M., and Sauer, U. (2012). Multidimensional optimality of microbial metabolism. Science *336*, 601–604.

Shoval, O., Sheftel, H., Shinar, G., Hart, Y., Ramote, O., Mayo, A., Dekel, E., Kavanagh, K., and Alon, U. (2012). Evolutionary trade-offs, Pareto optimality, and the geometry of phenotype space. Science *336*, 1157–1160.

Sourjik, V., and Wingreen, N.S. (2012). Responding to chemical gradients: bacterial chemotaxis. Curr. Opin. Cell Biol. *24*, 262–268.

Taute, K.M., Gude, S., Nghe, P., and Tans, S.J. (2014). Evolutionary constraints in variable environments, from proteins to networks. Trends Genet. *30*, 192–198.

Toker, A.S., and Macnab, R.M. (1997). Distinct regions of bacterial flagellar switch protein FliM interact with FliG, FliN and CheY. J. Mol. Biol. *273*, 623–634.

Toprak, E., Veres, A., Michel, J.B., Chait, R., Hartl, D.L., and Kishony, R. (2011). Evolutionary paths to antibiotic resistance under dynamically sustained drug selection. Nat. Genet. *44*, 101–105.

Typas, A., and Sourjik, V. (2015). Bacterial protein networks: properties and functions. Nat. Rev. Microbiol. *13*, 559–572.

Wang, X., and Wood, T.K. (2011). IS5 inserts upstream of the master motility operon *flhDC* in a quasi-Lamarckian way. ISME J. *5*, 1517–1525.

Weinreich, D.M., Delaney, N.F., Depristo, M.A., and Hartl, D.L. (2006). Darwinian evolution can follow only very few mutational paths to fitter proteins. Science *312*, 111–114.

Wilson, L.G., Martinez, V.A., Schwarz-Linek, J., Tailleur, J., Bryant, G., Pusey, P.N., and Poon, W.C.K. (2011). Differential dynamic microscopy of bacterial motility. Phys. Rev. Lett. *106*, 018101.

Wolfe, A.J., and Berg, H.C. (1989). Migration of bacteria in semisolid agar. Proc. Natl. Acad. Sci. USA *86*, 6973–6977.

Zarrinpar, A., Park, S.H., and Lim, W.A. (2003). Optimization of specificity in a cellular protein interaction network by negative selection. Nature *426*, 676–680.

Cell Reports, Volume *18*

Supplemental Information

Evolutionary Remodeling of Bacterial Motility Checkpoint Control

Bin Ni, Bhaswar Ghosh, Ferencz S. Paldy, Remy Colin, Thomas Heimerl, and Victor Sourjik

Supplemental Information

Evolutionary Remodeling of Bacterial Motility Checkpoint Control

Bin Ni, Bhaswar Ghosh, Ferencz S. Paldy, Remy Colin, Thomas Heimerl, Victor Sourjik

SUPPLEMENTAL FIGURES

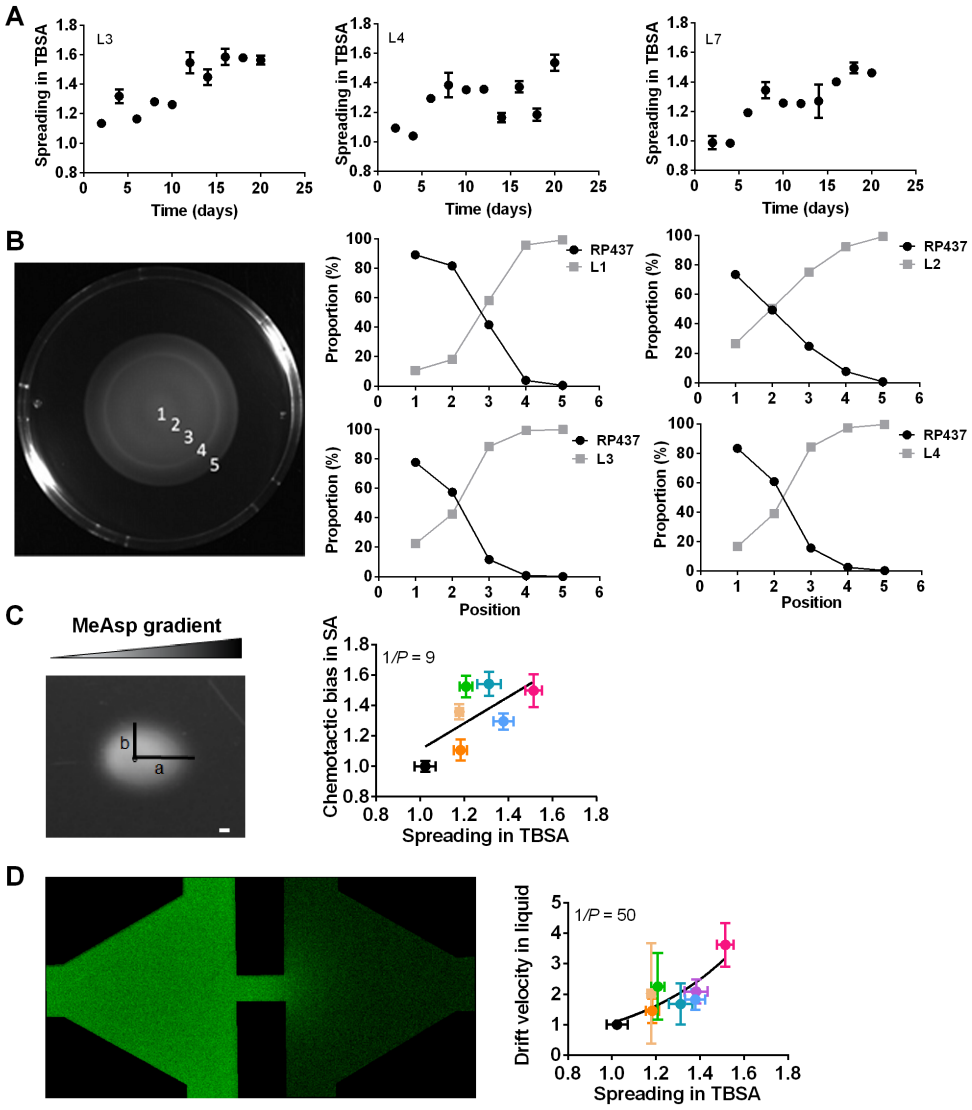

Figure S1. Experimental Evolution of *E. coli* Spreading and Its Characterization. Related to Figure 1. (A) Examples of time course of evolution of spreading in TBSA for lines L3, L4 and L7. **(B)** Competition assay in spreading between evolved strains and reference parental strain RP437. Evolved strains (labeled with CFP; pVS129) were co-inoculated 1:1 with RP437 (labeled with YFP; pVS132). Samples were collected at indicated positions along the colony spreading in TBSA (left panel) and fractions of both strains at each position were quantified using flow cytometry (right panels). Data in (A) and (B) are represented as mean ± SEM of three replicates. **(C)** Correlation between spreading in TBSA and biased movement (chemotactic bias) in minimal medium SA with pre-established gradient (0 - 100 μM) of MeAsp. Chemotactic bias was quantified as a ratio of spreading up the gradient to the spreading normal to the gradient (a/b). Scale bar is 1 mm. **(D)** Correlation between spreading in TBSA and chemotactic drift velocity in MeAsp gradient established in a liquid-filled PDMS chamber. Gradient formation in the microfluidic device was monitored using fluorescein. The channel dimensions are 2 x 1 mm. Correlation values are 0.65 (C) and 0.78 (D). Line in (D) indicates an exponential fit.

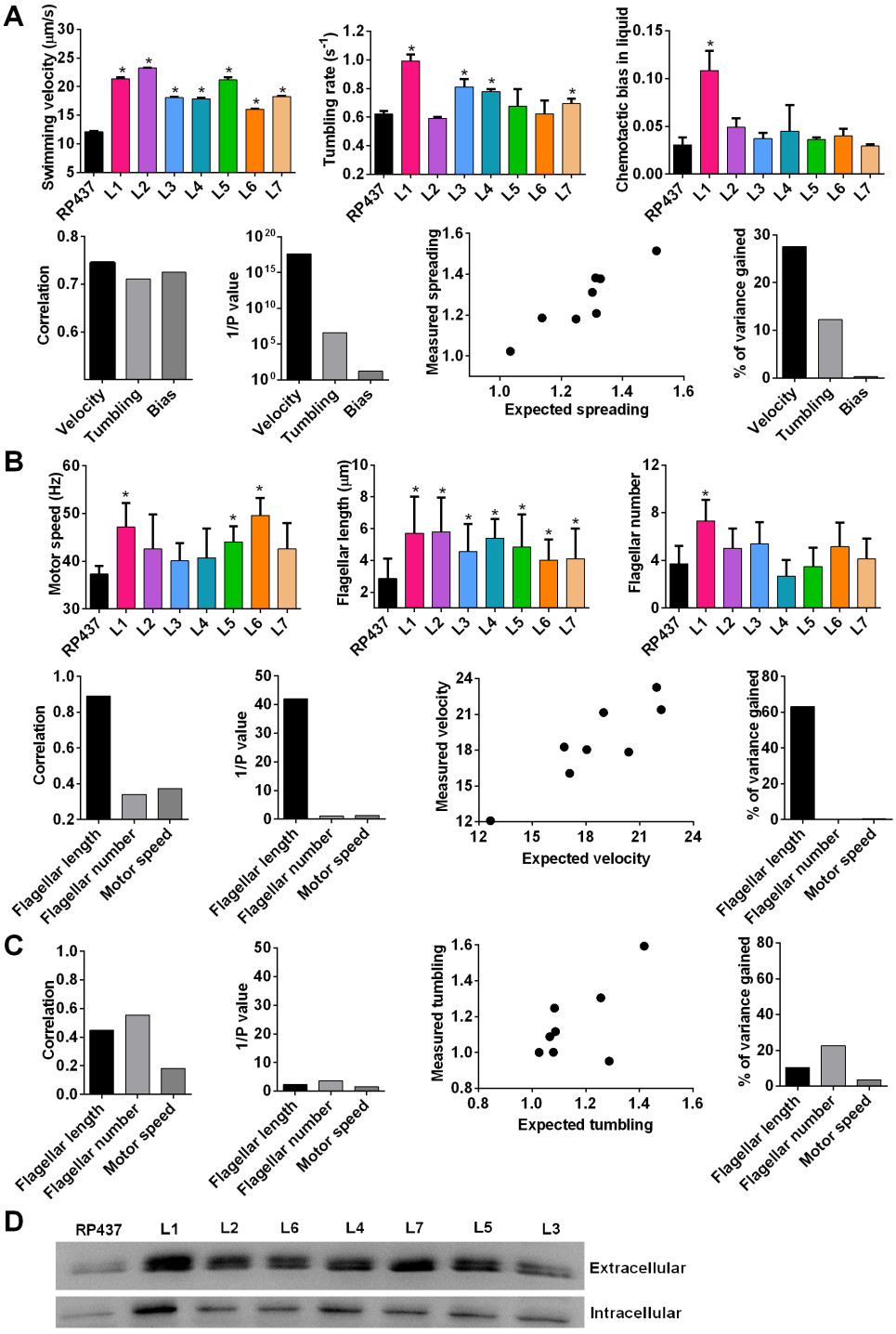

Figure S2. Regression Analysis of Correlation between Spreading, Motility and Flagellation in Evolved Strains. Related to Figure 2. (A) Correlation between spreading and velocity, tumbling rate and bias for motility analysis performed in liquid in absence of chemical gradients. Chemotactic bias in liquid was defined as chemotactic drift (Fig. S1D) normalized by cell swimming velocity. Asterisks indicate significant differences from PR437 according to two-tailed *t*-test ($P < 0.05$). Regression analysis was performed using linear regression model as described in the Supplemental Experimental Procedures. **(B)** Correlation between velocity and flagellar length, flagellar number and motor speed.

Rotation rate of individual flagellar motors in evolved cells was determined by tracking 1.1 μm beads attached to flagella. Electron microscopy was used to quantify flagellar length and number in evolved strains. **(C)** Correlation between tumbling rate and flagellar length, flagellar number and motor speed. **(D)** Western Blot analysis of flagellin levels inside and outside the cell for RP437 and evolved strains.

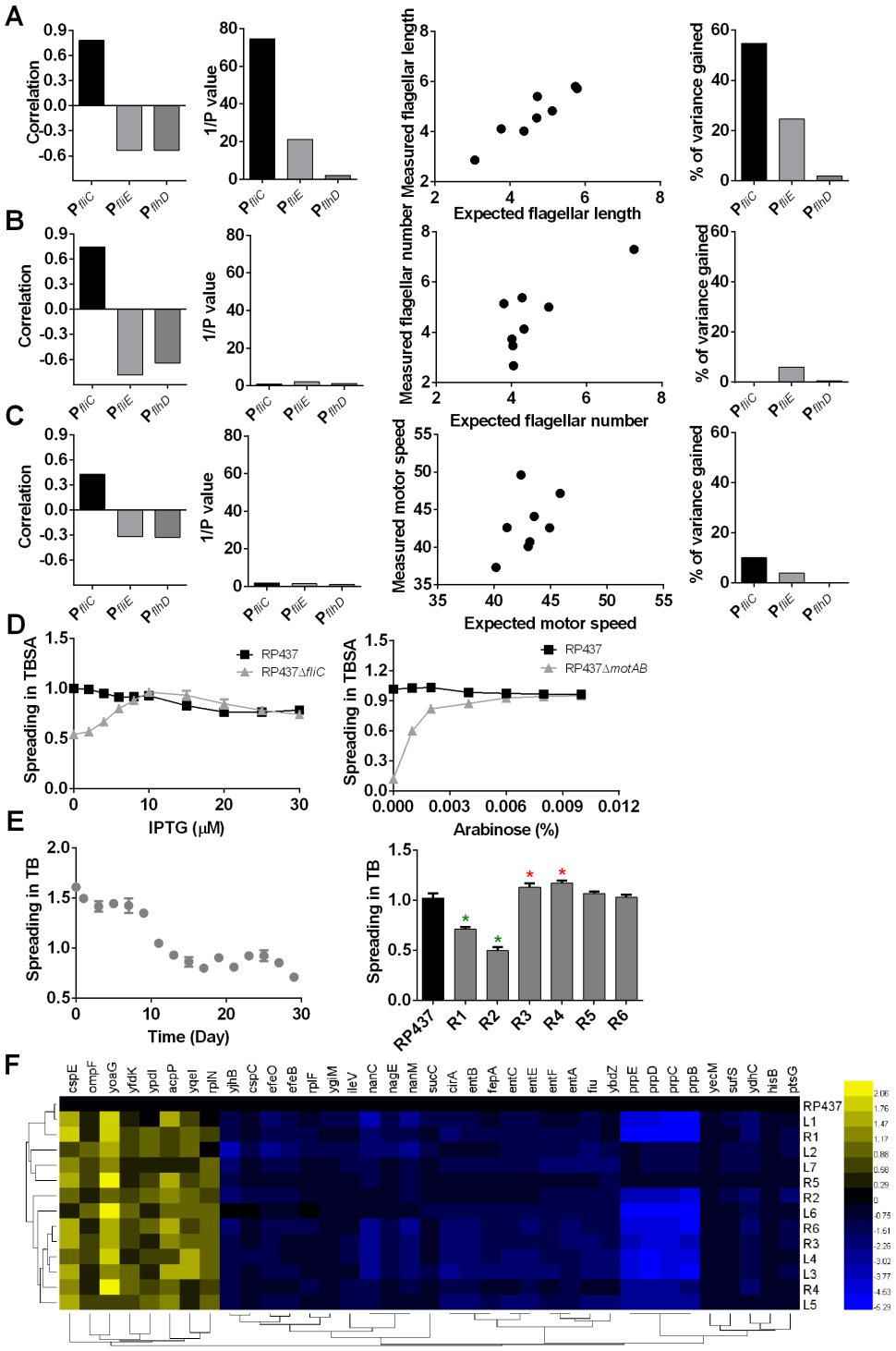

Figure S3. Changes in Gene Expression during Evolution. Related to Figure 2. (A-C) Regression analysis of correlation between flagellar length (A), flagellar number (B) or motor speed (C) and P_{fliC}, P_{fliE} or P_{flhD} promoter activities. Regression analysis was performed using linear regression model as described in the Supplemental Experimental Procedures. **(D)** Titration of FliC (left) or MotA and MotB (right) either in RP437 or in corresponding knockout strains. **(E)** Example of time evolution of spreading efficiency for L1 strain grown in liquid TB (left) and spreading efficiency after 20-30 rounds of selection for individual lines of evolution (right). Asterisks indicate significance for decrease (green)

or increase (red) in spreading compared to RP437 according to *t*-test ($P < 0.05$). Data in (D and E) are represented as mean ± SEM of three replicates. **(F)** Genes that changed their transcription independent of selection for motility according to the RNAseq analysis.

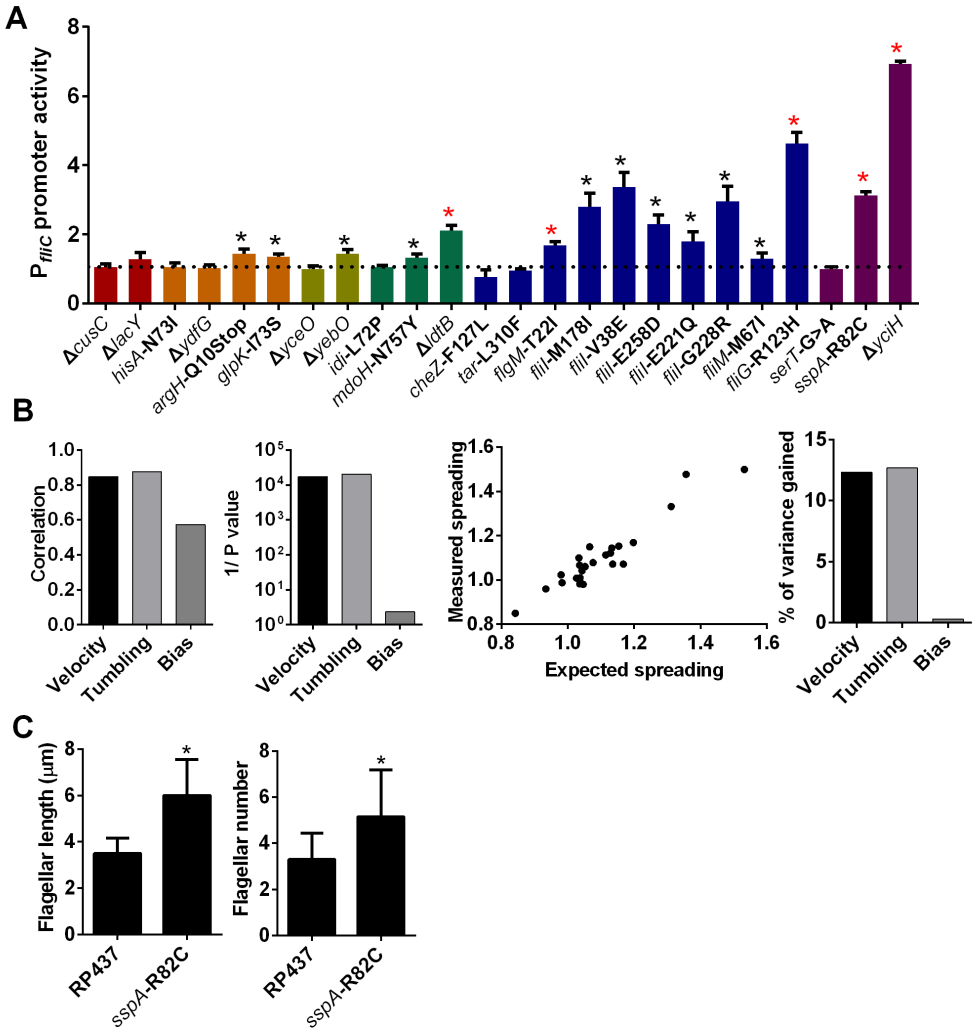

Figure S4. Analysis of Effects of Individual Mutations. Related to Figure 3. (A) P_{fliC} promoter activity for RP437 strain carrying individual adaptive mutations, normalized to RP437. Significant increase (black asterisks, $P < 0.05$; red asterisks, $P < 0.01$) in expression compared to the parental strain RP437 is indicated. **(B)** Regression analysis of correlation between spreading in TBSA and velocity, tumbling and chemotactic bias. Regression analysis was performed using linear regression model as described in the Supplemental Experimental Procedures. **(C)** Effects of R82C mutation in *sspA* on flagellar length and number. Asterisks indicate significant increase in number and length of flagella compared to RP437 according to *t*-test ($P < 0.05$). Data in (A and C) are represented as mean ± SEM of three replicates.

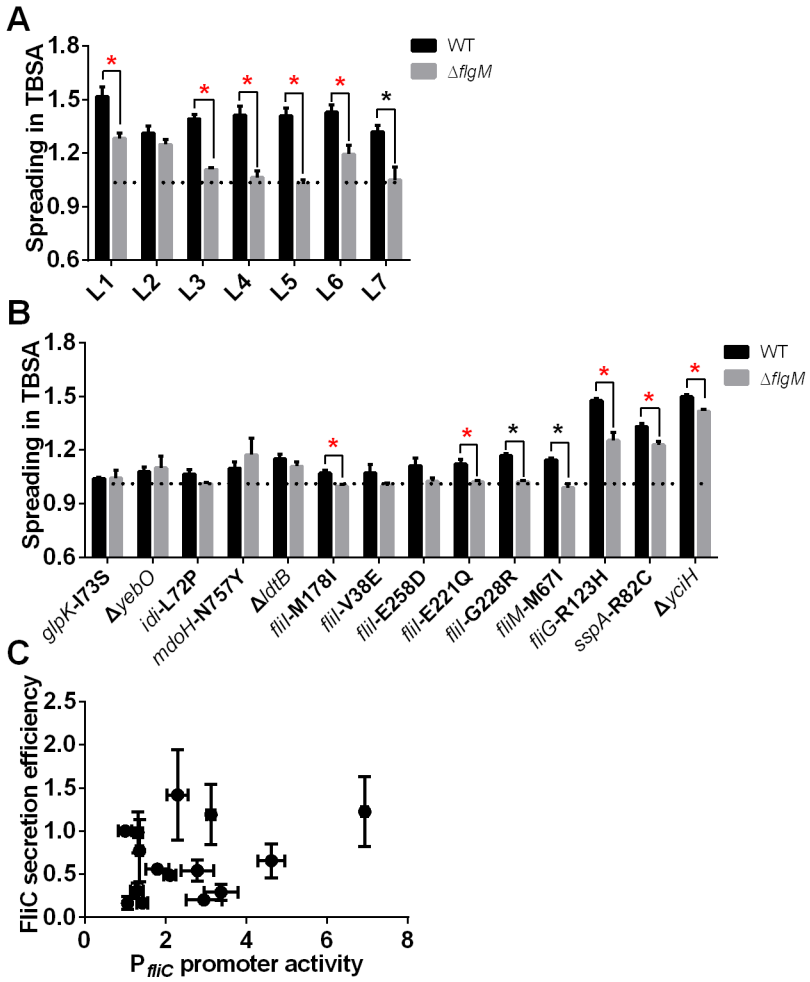

Figure S5. FlgM Secretion Controls on Spreading in TBSA. Related to Figure 4. (A,B) Spreading of evolved strains (A) or of RP437 carrying individual mutations (B), either in presence of FlgM (black bars) or in *flgM* knockout strain (grey bars). In each case, spreading was normalized to the respective reference strain, RP437 or RP437Δ*flgM*. Asterisks indicate significant difference between relative spreading in $FlgM^+$ and Δ*flgM* backgrounds (black: $P < 0.05$; red: $P < 0.01$) according to two-tailed *t*-test. (C) Correlation between FliC secretion efficiency and P_{fliC} promoter activity in strains containing individual mutation.

SUPPLEMENTAL TABLES

Table S1. Mutations Found in Evolved Strains by Genome Resequencing. Related to Figure 3.

Function	Genes	Annotation	L1	L2	L3	L4	L5	L6	L7
Motility	*fliI*	ATPase of flagellar export apparatus	E258D	M178I		G228R	V38E		E221Q
	fliM	flagellar motor switch protein	M67I						
	fliG	flagellar motor switch protein				R123H			
	tar	chemoreceptor		L310F					
	cheZ	phosphatase for CheY-P			F127L				
	flgM	anti-sigma factor for FliA			T22I				
Regulatory factor	*serT*	serine tRNA	C>T[a]						
	sspA	stringent starvation protein A	R82C						
	yciH	translation initiation factor		Q36Stop					
Cell envelope biogenesis	*ldtB*	L, D-transpeptidase						IS1	
	mdoH	membrane glycosyltransferase		N757Y					
	idi	isopentenyl diphosphate isomerase							L72P
Metabolism	*hisA*	L-histidine biosynthesis	N73I				N73I	N73I	
	argH	L-arginine biosynthesis		Q10Stop					
	glpK	glycerol kinase		I73S					
	ydfG	3-hydroxy acid dehydrogenase		IS1[b]					
Transporter	*cusC*	copper / silver efflux system		IS1					
	lacY	lactose permease	Del						
Unknown	*yebO*	unknown			IS1				
	yceO	possible regulator of biofilm formation / acid stress		IS1	IS1	IS1			IS1

[a]Mutation from guanine to adenine at position 31 in *serT* RNA.

[b]Insertion of transposable IS1 sequence.

Table S2. Mutations in Motility Genes Found in Strains Evolved in Minimal Medium. Related to Figure 7.

Genes	Annotation	Asp_1[a]	Asp_2	Ser_1	Ser_2	Glc_1	Glc_2	MA_1	MA_2
fliH	regulatory component of FliI				Q217H				H95L
fliI	ATPase of flagellar export apparatus	R231L	V301A	T377M		V70L	S106C		
fliM	flagellar motor switch protein							T192N	

[a]All lines were evolved in in Minimal A medium SA with 0.2% glucose as carbon source. Lines Asp_1, Asp_2, Ser_1 and Ser_2 were additionally supplemented with 1 mM aspartate or serine, respectively, as chemoattractant. For lines Glc_1 and Glc_2 glucose was both carbon source and chemoattractant. Lines MA_1 and MA_2 were evolved in a pre-established gradient of MeAsp (see Fig. S1C).

SUPPLEMENTAL EXPERIMENTAL PROCEDURES

Strains and Plasmid Construction

pKOV was used to integrate single SNP mutation into the genome of wild type strain (Link et al., 1997). Gene deletions were constructed by P1 transduction from KEIO collection (Baba et al., 2006). Kanamycin resistance cassette was removed using pCP20 (Cherepanov and Wackernagel, 1995). GFP reporters for *flhD* and *fliC* promoters were constructed based on pUA66 (Zaslaver et al., 2006), yielding pAM104 and pAM109, respectively. Promoter reporters for other genes were from a pUA66-based promoter library (Zaslaver et al., 2006). pTrc99a vector inducible by isopropyl β-D-1-thiogalactopyranoside (IPTG) was used to express FliA (pBN2), FlgM (pBN3), FlgM fused C-terminally to HA tag (pBN4) or FliC (pBN5). pBAD18-Kan vector inducible by arabinose was used to express MotAB (pBN6). pKAF131 carrying sticky *fliC* allele under native *fliC* promoter (Yuan et al., 2010) was a gift of Karen A. Fahrner and Howard C. Berg. For bead assay, *fliC* knockout strains carrying pKAF131 were used.

Immunoblot Analysis of FlgM or FliC Secretion

Cell cultures were adjusted to the same density (OD_{600} = 0.5-0.6) and centrifuged at 4,000 rpm for 8 min. Proteins in cell free supernatant were precipitated by 25 % trichloroacetic acid (TCA) and incubated on ice for 5 min. Precipitated proteins were collected by centrifugation (10,000 rpm) at 4 °C and washed twice with ice-cold acetone. After drying, 1X sample buffer containing 8 M urea was used to dissolve pellet for SDS-PAGE. Samples were separated on 15 % PAGE and transferred to PVDF membrane using wet blotting. Primary anti-HA antibody (Sigma) at a 1:10,000 dilution and secondary anti-mouse IgG antibody labeled with peroxidase (Sigma) at a 1:5,000 dilution were used for detection.

Regression Analysis

In order to asses relative contributions of individual independent variables on the dependent, we constructed a multilinear regression model, where the dependent variable (y) is assumed to be a linear additive function of the independent variables (x_1, x_2, x_3)

$$y = a_0 + a_1x_1 + a_2x_2 + a_3x_3$$

Linear least square method was used to calculate the values of coefficients. The value of R^2 gives an estimate of the proportion of variance of the dependent variable predictable from the full mutilinear regression model. Statistical significance of estimating each parameter of the model is measured by calculating the *p*-value of the *t*-statistics. The *p*-value of the parameter is the measure of the corresponding independent variable's relative contribution in predicting the dependent variable. The significance of the full model is calculated by estimating the *p*-value of the *F*-statistics of the full model. Since in the full model it is assumed that the independent variables are uncorrelated, we further constructed linear models where one of the independent parameters (x_1) is removed from the model so that the dependent variable is

$$y = a_0 + a_2x_2 + a_3x_3$$

and calculated R^2. The gain in R^2 by adding the variable is a measure of effect of the variable x_1 in explaining the variance of the dependent variable:

$$\Delta R^2(x_1) = R^2(fullmodel) - R^2(modelafterremovingx_1)$$

The values of ΔR^2 corroborate the significances calculated from the *p*-values of the full model. The calculations were performed using the *lm* function of the software *R*.

Spearman Rank Correlation(ρ)

The association between each pair of variables was calculated using Spearman rank correlation (ρ). The values of each variables were ranked and the correlation between the ranks was calculated. Since rank correlation does not assume any functional relationship between the variables, it is appropriate when the relationship is unknown. The corresponding significance of the correlation value was estimated by Spearman rho test which computes a probability of the correlation value being zero. The calculations were performed by the cor.test function of the software *R*.

Evolutionary Algorithm

Evolutionary simulations for topologies shown in Figure 7B were performed in MATLAB using standard genetic algorithm framework (Mitchell, 1998). Each simulation starts with a homogeneous population of 500 individual networks with the same topology and identical parameter values. In each generation, one of the model parameters is mutated randomly from a uniform distribution from 0 to 1 in each of the individual networks selected by the mutation rate 0.8 (i.e., in 80% of the networks). The I/O behavior of the network is modeled as a linear relationship. Thus, for the linear network with one input (x), one intermediate (y) and one output (z),

$$y = y_T w_1 x$$
$$z = z_T w_2 y$$

Here w_1 and w_2 denote the strength of the links between the input and the intermediate and between the intermediate and the output, respectively; y_T and z_T represent maximal attainable values of y and z, respectively, for one incoming link.

For the linear network with three inputs and three intermediates but one output,

$$y_1 = y_{1T} w_1 x_1; y_2 = y_{2T} w_2 x_2; y_3 = y_{3T} w_3 x_3;$$
$$z = z_T (w_4 y_1 + w_5 y_2 + w_6 y_3)$$

For the bow-tie network,

$$y = y_T (w_1 x_1 + w_2 x_2 + w_3 x_3)$$
$$z = z_T w_4 y$$

The fitness is defined to be proportional to the exponential of the output,

$$F = e^{(0.1+z)}$$

and it is calculated for each individual network in the population. Notably, in our model the maximal attainable fitness of the network is determined by the number of inputs that can acquire mutations, so that it is lower for a linear network with one input but the same for the linear and bow-tie networks with three inputs.

During *in-silico* evolution, the networks for the next generation are selected among the parental networks with replacement following proportional reproduction with the exponential scaling (Lampert and Tlusty, 2009; Burda et al., 2010; Friedlander et al., 2015). The fitness of the whole population is calculated as average fitness over the 500 networks. For each case the simulation was repeated for 100 different initial parameter sets so that evolution starts from a different point in the genotype space in order to avoid dependence on the initial parameter values. Median value of the fitness over these 100 different evolutionary runs was taken as a measure of the time trace of evolution.

SUPPLEMENTAL REFERENCES

Baba, T., Ara, T., Hasegawa, M., Takai, Y., Okumura, Y., Baba, M., Datsenko, K.A., Tomita, M., Wanner, B.L., and Mori, H. (2006). Construction of *Escherichia coli* K-12 in-frame, single-gene knockout mutants: the Keio collection. Mol. Syst. Biol. *2*, 2006.0008.

Burda, Z., Krzywicki, A., Martin, O.C., and Zagorski, M. (2010) Distribution of essential interactions in model gene regulatory networks under mutation-selection balance. Phys. Rev. E Stat. Nonlin. Soft Matter Phys. *82*, 011908.

Cherepanov, P.P., and Wackernagel, W. (1995). Gene disruption in *Escherichia coli*: Tc^R and Km^R cassettes with the option of Flp-catalyzed excision of the antibiotic-resistance determinant. Gene *158*, 9-14.

Friedlander, T., Mayo, A.E., Tlusty, T., and Alon, U. (2015) Evolution of Bow-Tie Architectures in Biology. PLoS Comput. Biol. 11, e1004055.

Lampert, A., and Tlusty, T. (2009) Mutability as an altruistic trait in finite asexual populations. J. Theor. Biol. 261, 414–422.

Link, A.J., Phillips, D., and Church, G.M. (1997). Methods for generating precise deletions and insertions in the genome of wild-type *Escherichia coli*: application to open reading frame characterization. J. Bacteriol. *179*, 6228-6237.

Mitchell, M. (1998). An introduction to genetic algorithms. Cambridge, Massachusetts, MIT Press.

Yuan, J., Fahrner, K.A., Turner, L., and Berg, H.C. (2010). Asymmetry in the clockwise and counterclockwise rotation of the bacterial flagellar motor. Proc. Natl. Acad. Sci. USA *107*, 12846-12849.

Zaslaver, A., Bren, A., Ronen, M., Itzkovitz, S., Kikoin, I., Shavit, S., Liebermeister, W., Surette, M.G., and Alon, U. (2006). A comprehensive library of fluorescent transcriptional reporters for *Escherichia coli*. Nat. Methods *3*, 623-628.